Physics Reports 802 (2019) 1–22

Contents lists available at ScienceDirect

Physics Reports

journal homepage: www.elsevier.com/locate/physrep

The geometry of cutting and shuffling: An outline of possibilities for piecewise isometries

Lachlan D. Smith [a,b], Paul B. Umbanhowar [c], Richard M. Lueptow [b,c,d], Julio M. Ottino [b,c,d,*]

[a] School of Mathematics and Statistics, The University of Sydney, Sydney, New South Wales 2006, Australia
[b] Department of Chemical and Biological Engineering, Northwestern University, Evanston, IL 60208, USA
[c] Department of Mechanical Engineering, Northwestern University, Evanston, IL 60208, USA
[d] Northwestern Institute on Complex Systems (NICO), Northwestern University, Evanston, IL 60208, USA

ARTICLE INFO

Article history:
Received 18 January 2019
Accepted 18 January 2019
Available online 28 February 2019
Editor: D.K. Campbell

ABSTRACT

Cutting and shuffling is emerging as an alternative mixing mechanism for fluids and granular matter beyond the well established stretching and folding. Dynamical systems and chaos theory provided a foundation for stretching and folding which has led to applications ranging from microfluidic devices and physiological scales to many engineering and Earth science scales. Likewise, the literature of piecewise isometries (PWIs) provides a similar grounding for cutting and shuffling mechanisms. We start with one-dimensional interval exchange transformations (IETs), which are the only way to cut and shuffle in one dimension, and review and extend previous studies, connecting them in a coherent way. We introduce the concept of time-continuous piecewise isometries, i.e. PWIs that can be performed on solid bodies in a time continuous manner, without solids overlapping or the domain needing to be deformed or extended. PWIs with this property are easier to implement in experiment and applications, as we demonstrate through their connection to mixing in spherical granular tumblers and "twisty puzzles," such as the spherical version of the Rubik's cube.

Contents

* Corresponding author at: Department of Chemical and Biological Engineering, Northwestern University, Evanston, IL 60208, USA.
E-mail addresses: lachlan.smith@sydney.edu.au (L.D. Smith), umbanhowar@northwestern.edu (P.B. Umbanhowar), r-lueptow@northwestern.edu (R.M. Lueptow), jm-ottino@northwestern.edu (J.M. Ottino).

https://doi.org/10.1016/j.physrep.2019.01.003
0370-1573/

1. Introduction

Interval exchange transformations (IETs) and their higher dimensional generalizations, piecewise isometries (PWIs) fall in the fortunate class of abstract mathematical concepts that turn out to have applications in areas of practical importance. Earlier works have noted applications to digital filters [1–4] and "kicked" Hamiltonian mappings [5,6]. Here we bring in another area: mixing of fluids and, surprisingly, granular matter. The objective of mixing is to bring together two or more initially segregated materials, increasing the degree of interspersion by creating interfacial area between them, and driving the system towards a homogeneous state. In fluids, where the elements are atoms or molecules, mixing can be achieved by turbulence or, more deliberately, by the stretching-and-folding mechanisms of chaotic flows [7]; if the fluids are miscible, thermal diffusion drives mixing at the smallest length scales. In bulk solids composed of macroscopic (athermal) particles, the particles can be deliberately rearranged, as in the cutting-and-shuffling of a deck of cards. Stretching-and-folding can be couched in the language of dynamical systems. But there is also a very physical connection between a horseshoe map and realizing one in the lab with an actual fluid. Cutting-and-shuffling is becoming a second paradigm for mixing and, conveniently, can be couched in the language of IETs and PWIs. The physical connection is immediate.

IETs are maps that cut and shuffle a one-dimensional (1D) line interval. They can be traced back to the work of Keane [8,9], which gave criteria for an IET to be "minimal", in a sense, mixing. Other studies have since built on Keane's work [10–24]. For instance, Avila and Forni proved that almost all IETs satisfying Keane's minimality condition are "weak-mixing" [19]. While the definition of an IET is simple, their dynamics are surprisingly complex, and the study of IETs is still active.

PWIs are the natural generalization of IETs to higher dimensional domains. A PWI is a map $M : X \to X$ such that X is cut into a number of pieces that are rearranged and reassembled to recover the original domain X. "Piecewise" means that a different action is performed on each cut piece, and "isometry" means the map on each piece is length-preserving (e.g. translation, rotation, reflection, screw motion), such that no stretching occurs. Much of the seminal work can be traced back to Goetz and Ashwin [2,3,25–36]. Since then, PWIs have found application in granular mixing [13,37–45], and cutting-and-shuffling combined with stretching-and-folding can be used to mix fluids [46–62].

With mixing as the underlying theme, the present paper reviews and ties together earlier studies on IETs and PWIs, connecting them in a coherent manner. In doing so we generalize and define broader classes of PWIs, such as the concept of lune exchange transformations, and time-continuous PWIs, which we use to link to physical systems such as the biaxial spherical tumbler (BST) flow [13,37–45] and twisty puzzles (e.g., the Rubik's cube). Definitions are introduced in order to link areas and studies serving to connect somewhat disjointed PWI studies, as well as outlining directions for future research (e.g., fully three-dimensional (3D) PWIs).

Framing Questions

When discussing cutting and shuffling motions it is important to consider the following:

- Can the motion be performed on solids, either theoretically or experimentally, without deforming or extending the domain? Consider, for example, the PWI shown in Fig. 1, where two elephants are cut out, one red and one white, and their positions are swapped. Imagining the domain as a 2D solid square (like cookie dough), in order to move the elephants to their new positions it is necessary to pick them up, out of the 2D square domain, i.e. the domain needs to be extended to three dimensions. Similarly, for split-and-recombine mixers [51–59], such as the design shown in Fig. 2, where a single channel divides into multiple sub-channels, in order for the channels to recombine in a non-trivial way, the cross-sectional shape must change, both extending and deforming in shape. In contrast, the spherical version of the Rubik's cube, shown in Fig. 3, can be scrambled using cutting-and-shuffling, and the shape of the domain does not change. It remains spherical regardless of the action performed.
- What type of discontinuous deformation can result from the continuous isometric motion? Is it a cut-and-shuffle in the traditional sense, like shuffling a deck of cards, or the map shown in Fig. 1? Or does one surface slide over another, yielding a "slip" deformation, like twisting a spherical cap of the Rubik's sphere (Fig. 3), or layers of earth sliding over one another in a thrust fault [63–65]? This is the difference between "cutting" and "sliding" singularities defined by Kahng [66].
- Is the motion orientation preserving, i.e. does it contain a reflection that would make it orientation reversing? For example, what happens if one of the elephants in Fig. 1 is facing left instead of right requiring both elephants to be flipped when they are exchanged?

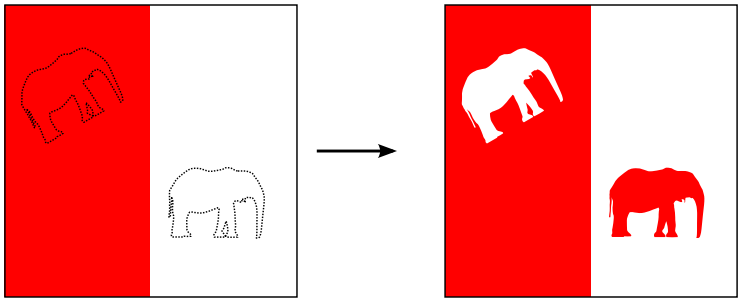

Fig. 1. Demonstration of an arbitrary cut-and-shuffle action, cutting the same shape from two different positions and swapping them. It is impossible to parametrically study these types of PWIs because it is impossible to consider every possible shape.

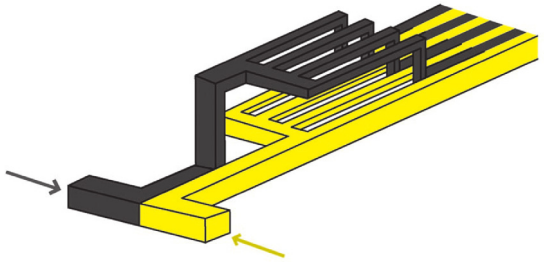

Fig. 2. Mixing fluids by splitting a channel into multiple sub-channels and recombining them.
Source: Adapted with permission from Sudarsan et al., "Multivortex Micromixing", *Proc. Natl. Acad. Sci. USA* **103**(19), 2006 [59].

Fig. 3. The Rubik's sphere operates identically to the standard $3 \times 3 \times 3$ Rubik's cube ©User:SpinningSpark/Wikimedia Commons/CC-BY-SA-3.0. Cutting and shuffling is generated by rotating spherical caps, which creates "slip" deformations, but the rotated piece remains entirely within the spherical domain.

To address the first question, we introduce the concept of PWIs that can be represented as time-continuous motions. That is, can the PWI, $M : X \to X$, which is a time-discrete map, be transformed into a time-continuous map $M' : X \times [0, 1] \to X$, where $M'(x, 0) = x$, $M'(x, 1) = M(x)$, and $M'(\cdot, t) : X \to X$ is a piecewise isometry for all $0 \leq t \leq 1$? The new parameter t can be thought of as a time variable that converts the time-discrete map into a time-continuous motion. Since the time-continuous map $M'(\cdot, t) : X \to X$ is a PWI for each t, pieces are prohibited from overlapping one another at any given time. As such, the domain does not need to be extended. As an example, consider the map $R_\alpha : D \to D$, which rotates a single unit disk D by α, i.e. $R_\alpha(r, \theta) = (r, \theta + \alpha)$ in polar coordinates. This time-discrete map can be expressed as the time-continuous map $R'_\alpha : D \times [0, 1] \to D$, where $R'_\alpha(r, \theta; t) = (r, \theta + t\alpha)$. The map R'_α satisfies $R'_\alpha(r, \theta; 0) = (r, \theta)$, $R'_\alpha(r, \theta; 1) = R_\alpha(r, \theta)$, and $R'_\alpha(\cdot, t) : D \to D$ is a PWI of D for all $0 \leq t \leq 1$. As we will show, this rotation, which is a simple, easily parameterizable (center and radius of disk, angle of rotation), time-continuous PWI, can be implemented physically. Furthermore, when two disks with different centers are overlapped and rotations are coupled, complex transport phenomena occur.

Structure of this work

This paper is an outline of possibilities and an attempt to provide a first draft of possible PWIs, ranging from 1D, 2D planar, 2D spherical, and 3D geometries, some of which may be experimentally realized. The presentation is anchored on

two concepts. One is seeing higher dimensional cutting and shuffling motions as extensions of one-dimensional interval exchange transformations (IET). The other is the concept of time-continuous piecewise-isometries, i.e. PWIs that can be performed on solid bodies in a time-continuous manner, without solids overlapping or the domain needing to be deformed or extended. The overall objective is to provide a structure that may lead to further insight, extensions, and possibilities. It is conceivable that a classification could be anchored on a sole, general, complete, and extensible mathematical basis, one that could allow for proofs and clear limits of what is and is not possible, i.e. limits guaranteed by theorems. However, with the exception of 1D IETs, and aspects of 2D rectangle exchange transformations, we are not there yet. In any case, mathematical terminology is needed to anchor the presentation and some of those aspects appeared in the opening sections of this work. The reader will note in what follows – a presentation of cases, roughly ordered in increasing order of complexity – an absence of definitive theorem-like wordings and statements, such as "the only possible", instead finding phrasings such as "may be possible" or "it appears that". Further, we will occasionally use physical explanations or even metaphors to explain the possible physical realizability of the systems proposed.

Let us consider now some of the issues facing us.

The current literature focuses primarily on orientation preserving PWIs (no reflections). It is not clear whether reflections would significantly change the transport and mixing characteristics of PWIs. It is important to recognize that, from a practical standpoint, in most cases reflections are impossible to perform as a time-continuous PWI. It is generally necessary to extend the domain to higher dimensions for a reflection. Using the 1D line interval as an example, reflections of a subsegment of the line interval can only be achieved by considering the line in the 2D plane and rotating the subsegment of the line through 180° in the 2D plane. Similarly, by considering a 2D planar shape, reflections can only be achieved by out-of-plane 180° rotations in 3D. However, if the geometry of the domain is already 3D, e.g. a sphere, then reflections require passing into the fourth dimension, making them physically impossible. Examples where orientation-reversal is possible are pulsed source–sink type systems [48–50,67–76], where fluid is extracted from one point and reinjected at another point. In these studies, fluid particles are generally reinjected along the same streamline that they are extracted from, making the flow orientation preserving. However, if the particles are reinjected on a reflected streamline, as considered by Lester et al. [68], the flow becomes orientation-reversing. In essence, the 2D domain itself is made to be non-orientable, like the Möbius strip. In the classification of PWIs presented here, we consider only orientation preserving isometries (translation, rotation, screw motion), but not reflections. Note also that the composition of any two orientation reversing isometries (reflections) is orientation preserving, so if M is an orientation reversing PWI, then M^2 is orientation preserving. Complications only arise when a PWI is partially orientation preserving and partially orientation reversing, i.e. some of the cut pieces are reflected, whereas others are not.

We also restrict our classification to PWIs that are easily parameterizable. These systems can be easily tuned to yield a desired outcome (e.g. optimal mixing). Consider, as an example of cutting-and-shuffling that is difficult to parameterize, cutting some arbitrary shape out of the 2D square in one location, then cutting the same shape out of the square in another location, and swapping the two shapes, as illustrated by the elephants in Fig. 1. The choice of an elephant shape is arbitrary, and it is impossible to parameterize *every* possible shape that can be cut out, making it impossible to parametrically study transport and mixing phenomena. The example in Fig. 1 also demonstrates the difficulty of reflections. If one of the shapes were reversed (one elephant faces to the left instead of the right), a reflection would be necessary. That is, both of the elephants would need to be rotated by 180° out of the plane of the domain to reassemble the square.

We categorize PWIs in different geometries by the dimensionality of their transport, i.e. are tracers confined to curves (1D) or surfaces (2D), or can they explore volumes (3D)? We also consider whether higher dimensional PWIs are extensions of lower dimensional PWIs, i.e. whether there is a natural embedding (isometric, one-to-one map) of the lower dimensional PWI into higher dimensional space. Examples of such embeddings include embedding 1D line intervals into 2D squares, which themselves embed into 3D cubes, or embedding 1D circles into 2D disks, which embed into 3D spheres. As we will show, when these embeddings exist, it is necessary to break geometric symmetries in order to generate higher dimensional transport. For example, overlapping two disks with different centers breaks the rotational symmetry of each disk.

A possible classification

A summary of our classification and the relationships between PWIs in different geometries is shown in Fig. 4. Natural embeddings are indicated by arrows, and classes that can be represented as time-continuous PWIs have a box around their name. Note that all the time-continuous PWIs are extensions of 1D circle rotations, whereas the others are extensions of 1D interval exchange transformations. We acknowledge that there may be other ways to classify PWIs, which may be more useful in other contexts. In addition, there are other PWIs to be classified (e.g. arbitrary cut-and-swaps like in Fig. 1), which can be added to Fig. 4. The paper is organized as follows, starting from 1D PWIs (circle rotations and interval exchange transformations), we discuss each class of PWI, following the general layout of Fig. 4. For each class, we discuss its relationships with other PWI classes, as well as general transport properties, and, where possible, physical implementations.

In Section 2 we explore cutting and shuffling motions in 1D, on the line interval and the circle, where *circle rotations* and *interval exchange transformations* are the only PWIs. Then, in Section 3 we consider planar and spherical 2D geometries. Interval exchange transformations naturally embed into both planar and spherical geometries as *rectangle exchange transformations* (discussed in Section 3.1), *overlapped planar wedge exchange transformations* (discussed in Section 3.3), and *multi-axis lune exchange transformations* on the sphere (discussed in Section 3.5). A special sub-class of

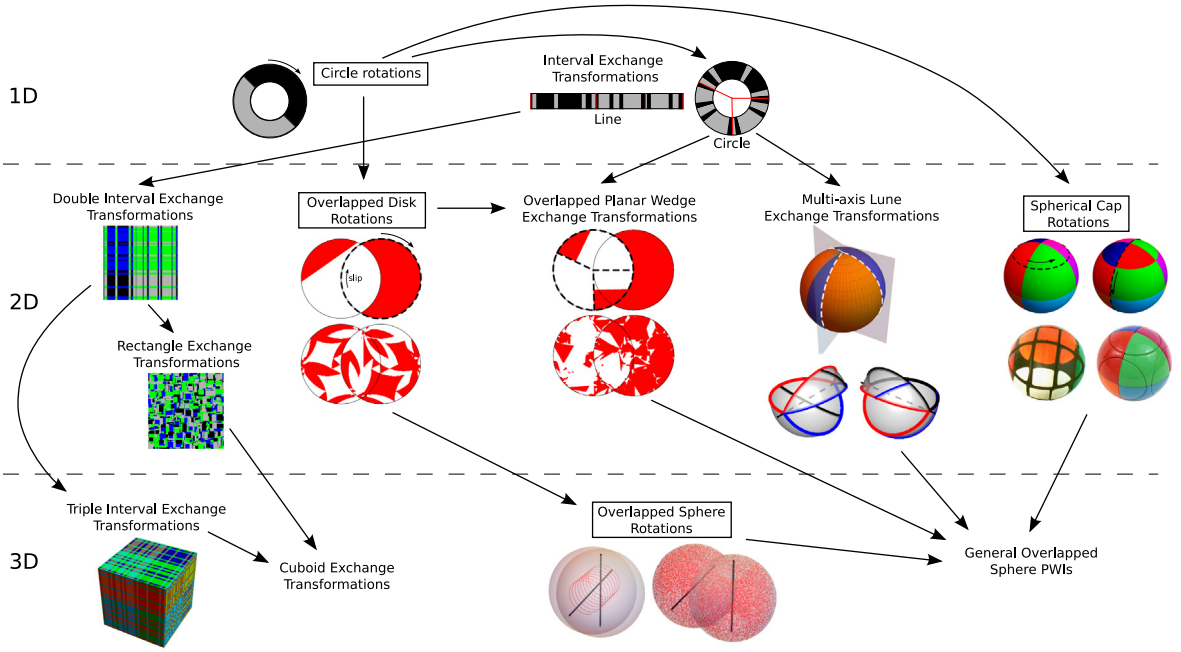

Fig. 4. Classification of PWIs in 1D, 2D, and 3D geometries. Arrows indicate natural extensions, known as embeddings. Classes with a box around their name are time-continuous PWIs, which all extend from rotations of a 1D circle. These PWIs can be implemented, theoretically and in some cases experimentally, to cut-and-shuffle solids without modifying the shape of the domain in the process, e.g. the Rubik's sphere in the "Spherical Cap Rotation" class. Non-time-continuous PWIs are natural extensions of 1D interval exchange transformations, which are the most general form of PWIs in one dimension.

planar wedge exchange transformations are *disk rotations*, which are the only planar wedge exchange transformations that can be represented as time-continuous PWIs of the plane. When two (or more) disk rotations are overlapped, interesting 2D transport and mixing results, which is discussed in Section 3.4. In a spherical geometry, *spherical cap rotations* (discussed in Section 3.6) provide another basic piecewise-isometric motion, which extend from 1D circle rotations and can be represented as time-continuous PWIs of the sphere. Next, we explore three-dimensional cutting and shuffling in Section 4. In Section 4.1, we discuss the natural extensions of 1D interval exchange transformations and 2D rectangle exchange transformations to 3D *cuboid exchange transformations*. In Section 4.2, we show that performing 2D spherical PWIs alternately on two overlapped spheres provides a general method to create three-dimensional transport by cutting and shuffling. We discuss the simplest case, where two overlapped spheres alternately undergo solid body rotations (*overlapped sphere rotations*), and show that the orientations of the rotation axes play an important role in the dimensionality of tracer transport. As for overlapped disks discussed in Section 3.4, these overlapped sphere rotations can be represented as time-continuous PWIs. Lastly, we summarize our results and offer concluding remarks in Section 5.

2. One-dimensional cutting and shuffling

2.1. Interval exchange transformations

We begin with the 1D line interval, where only translations are possible. In 1D, the only orientation-preserving PWIs are interval exchange transformations (IETs), where the line interval is cut into a number of pieces at the same location for each iteration, and the pieces are rearranged (translated) according to a permutation, π, as shown in Fig. 5(a) for the permutation $\pi = 321$. Note that the IETs are shown with finite line width only to make the colors more easily visible, even though they actually have zero line width. While IETs may seem simple, they give rise to complex behavior, and have been studied extensively [8–24]. Depending upon the locations of the cuts and the rearrangement permutation, the black and gray colors may mix, as shown for iteration $N = 10$ in Fig. 5(a), or the colors may reassemble back to their initial configuration ($N = 0$). If the cuts occur at rational points along the line interval (rescaled to have length equal to one), then the line interval can be cut into a finite number of equal-length segments, and the map will never sub-divide any of those segments, independent of how many iterations are performed. Effectively, the domain is spatially discrete. For example, consider cutting a deck of cards after the 10th and 42nd cards to create three piles, then swapping the top pile with the bottom pile. This action can be repeated indefinitely, and it will never be necessary to cut a card in half. In fact, it is guaranteed that after 52! iterations, or some smaller divisor of 52!, the deck will return to its original state.

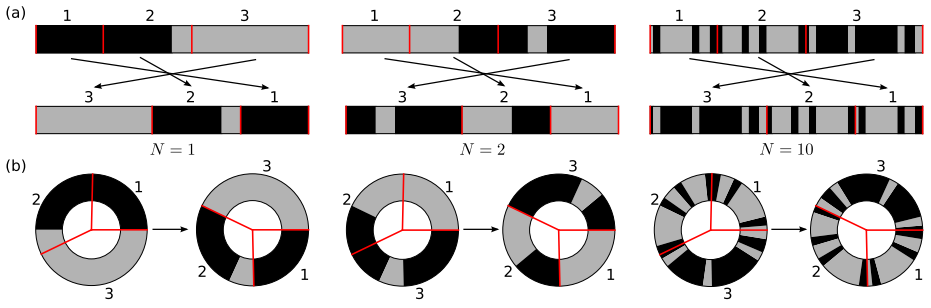

Fig. 5. Interval exchange transformation on (a) the line interval, and (b) the circle, initially colored half black and half gray. Cutting lines are shown as red. At each iteration, the domain (line or circle) is cut at the same locations into three pieces, which are rearranged according to the permutation $\pi = 321$. After $N = 10$ iterations, the black and gray colors are more mixed.

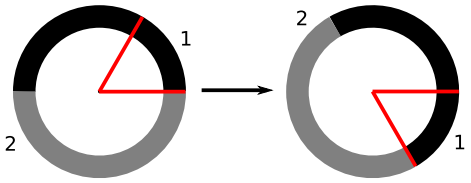

Fig. 6. The IET that cuts the circle into two pieces and then rearranges them according to the permutation $\pi = 21$ effectively rotates the circle. This demonstrates the embedding of circle rotations into circle IETs, shown by the connecting arrow in Fig. 4.

Similarly, any IET with all cuts at rational points will be periodic. In the general setting, where cuts can occur anywhere along the line, IETs under appropriate conditions eventually cut the line into arbitrarily small segments. For example, repeating the IET in Fig. 5(a), which has cuts at irrational points along the line interval, will result in smaller and smaller black and gray segments. This is because it satisfies the Keane minimality condition [8,9,15] and hence is "weak-mixing".

Practical limitations

In general it is not possible to describe the motion of the entire line interval as a time-continuous PWI, because segments must cross over one another. For example, in the first iteration of Fig. 5(a), the piece labeled "1" must move past the "2" and "3" pieces to the end of the line, while piece "3" must move in the opposite direction to the front of the line. Like trains queued up on a single track, attempting to move in opposite directions, the pieces would collide. For an IET to be performed as a time-continuous piecewise-isometric motion, it is necessary to embed the line into two-dimensions so that segments can be moved vertically, out of the line, before they are moved horizontally past one another without colliding. This is akin to the use of railway sidings on single track lines that enable trains traveling in opposite directions to pass one another.

2.2. Circle rotations

If the ends of the line interval are "glued" together (a periodic boundary condition), then the line is topologically equivalent to a circle. Translations along the line can be viewed as rotations about the center of the circle. Fig. 5(b) shows the same IET as Fig. 5(a), but on the circle instead of the line. Again, pieces must move past other pieces to accomplish the rearrangement, requiring a second dimension analogous to the railway siding. A special, somewhat trivial, class of IETs are those that cut the circle into two pieces, and rearranges them according to the permutation $\pi = 21$, as demonstrated in Fig. 6. This type of IET simply rotates the circle clockwise through some angle, θ, which is the angle of the first piece. Therefore, circle rotations embed into circle IETs, shown by the connecting arrow in Fig. 4. Circle rotations cannot really be considered cutting-and-shuffling, because the circle looks essentially the same after mapping, only rotated. However, they are the only IETs that are time-continuous PWIs.

Practical implementations

Returning to the analogy of trains on a single track, if the track forms a loop then all the trains can move in the same direction without collision. When the angle of rotation is incommensurate with π such rotations are ergodic, but not mixing, and when the angle is a rational multiple of π the rotation is periodic. This seemingly trivial class of IETs will play an important role in Sections 3.4 and 4.2. This is primarily because they are time-continuous PWIs, and hence can be theoretically, and in some cases practically, applied to solids.

A practical implementation of the circle rotation PWI is the Kenics static mixer [77–80] in which helical flutes within a cylindrical pipe rotate a viscous fluid flowing through the pipe, as shown in Fig. 7. In this case, the circle has non-zero

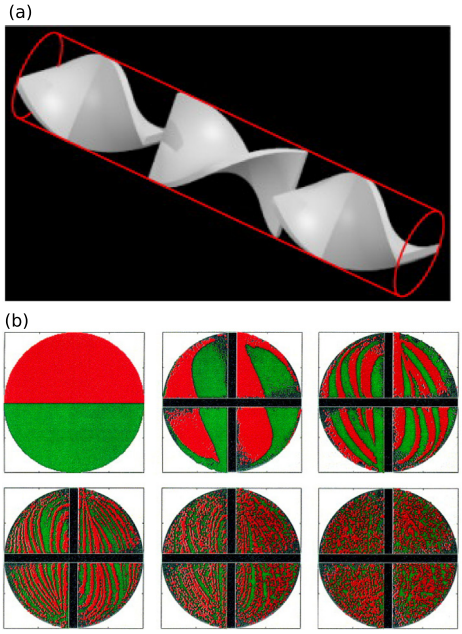

Fig. 7. (a) The Kenics static mixer [77–80] consists of helical flutes within a cylindrical pipe. Adapted with permission from Saatdjian et al., Chemical Engineering Journal, **187**, pp. 289–298 (2012) [80]. ©2012 Elsevier. As fluid flows through the cylindrical pipe, it is cut, rotated, stretched, and folded, leading to rapid mixing, as shown by the mixing of red and green colors in the cross-sections in (b). Adapted with permission from Hobbs and Muzzio, Chemical Engineering Journal, **67**(3), pp. 153–166 (1997) [79]. ©1997 Elsevier.

width, extending radially to the center of the circle. As well as rotating, the no-slip boundary conditions at the pipe wall and at the surfaces of the helical flutes lead to stretching and folding of the fluid. This stretching and folding then results in rapid mixing.

3. Two-dimensional cutting and shuffling

3.1. Double interval exchange transformations

There are two natural ways to extend 1D IETs to two dimensional planar geometry. They are shown by the two embeddings into planar geometries in Fig. 4, and relate to "trivial embeddings" of IETs into PWIs [81]. The first extension is from the 1D line to the 2D square. An IET can be performed in the horizontal direction, cutting the square into vertical strips and rearranging them, as demonstrated by the map from Fig. 8(a) to Fig. 8(b), followed by a second IET in the vertical direction, cutting the domain into horizontal strips and rearranging them, as demonstrated by the map from Fig. 8(b) to Fig. 8(c). The collection of these "double IETs" is a subclass of general rectangle exchange transformations (RETs) [82], and they have similar control parameters to IETs: the horizontal and vertical cut locations and the permutations used to rearrange the strips. In terms of mixing, it is likely that the resultant RET will inherit many of the properties (e.g. ergodicity, weak-mixing) from its parent IETs. An important caveat, however, is that transport is always limited. For example, using the 4-color quadrant initial condition shown in Fig. 8(a), an infinitesimally thin slice in either the vertical or horizontal directions can never contain all four colors using double IETs. This can be explained by considering the map on the grid or rectangles shown in Fig. 8(e–g). Looking at the first row of Fig. 8(e), it contains the numbers 1, 2, 3. The horizontal IET rearranges the numbers to 3, 2, 1, and the vertical IET moves the entire row down to the third row. However, it is impossible for any other number than 2 or 3 to be on the same row as 1, because the IETs always rearrange entire rows or columns. The numbers in each row or column may be permuted and the row or column translated to a new position, but no new numbers can ever join a row or column.

Practical limitations

Similar to IETs, the sequence of translations cannot be performed as time-continuous motions without rectangular pieces crossing over each other. Unlike 1D IETs, where it is necessary to extend the domain to two dimensions, RETs only require additional two-dimensional space in the plane of the rectangle for the time-continuous motion to occur (translating each column or row in this plane). RETs can be realized in practice if vacant space in the plane is allotted for cut pieces to move into. For example, "sliding block" puzzles such as the "15-puzzle" and "Rush Hour", where pieces can slide into vacant spaces, are examples of RETs. This is an important point for continuous flow channel mixers with

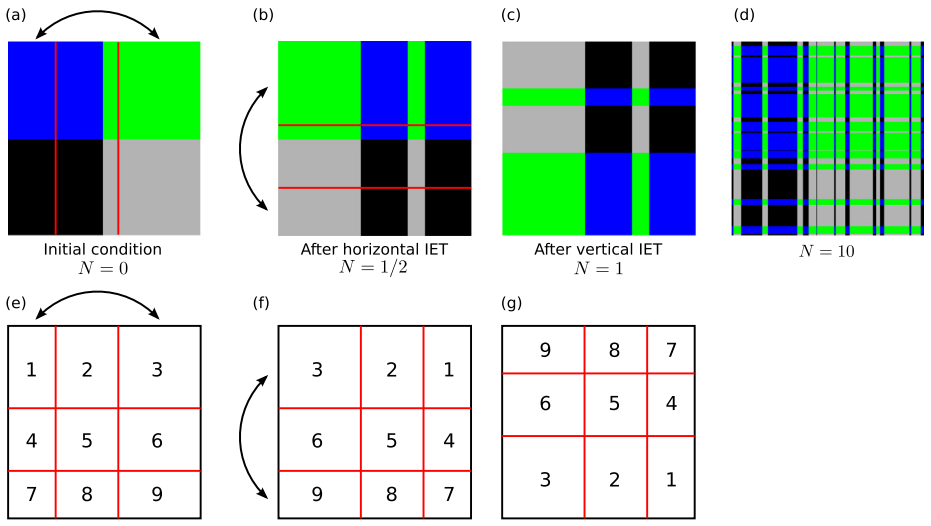

Fig. 8. Double IET, a type of rectangle exchange transformation (RET), consisting of an IET in the horizontal direction, mapping (a) to (b), and an IET in the vertical direction, mapping (b) to (c). The IET used in each step is the same as in Fig. 5(a). (d) After 10 iterations the colors are more mixed, but each vertical slice still contains only blue and black, or green and gray. Similarly, each horizontal slice contains only ever blue and green, or black and gray. (e–g) Each iteration of the double IET rearranges the nine rectangles shown in (e) resulting in (g).

periodic channel segments. Flow in such mixers is often modeled as a 2D time-dependent flow on cross-sectional slices, and the transport of tracers from the cross-section of one channel segment to the equivalent cross-section in the next channel segment defines a 2D map. If the periodic channel segments split and then recombine [51,53–59], as occurs in Fig. 2, then 2D cutting-and-shuffling, as an RET, takes place (along with stretching-and-folding). When the channel splits into sub-channels, the sub-channels must separate and twist around each other before recombining.

3.2. General double interval exchange transformations — Rectangle exchange transformations

A more general class of double IETs are those that perform different horizontal IETs on different horizontal strips, and likewise for the vertical IETs. For example, in Fig. 9(a), the square is cut into three horizontal strips, and a different IET is performed on each horizontal strip [Fig. 9(a) mapping to Fig. 9(b)]. The first two strips use the same permutation to rearrange the pieces, $\pi = 321$, but they have different cut locations, and the third strip uses a different permutation, $\pi = 51432$, and different cut locations (and more cuts). Next, a similar procedure takes place in the vertical direction, cutting the square into three vertical strips, and applying a different vertical IET to each strip [Fig. 9(c) mapping to Fig. 9(d)]. Note that after 10 iterations [Fig. 9(e)], mixing of the colors using this general double IET is significantly better than for the double IET shown in Fig. 8(d). In particular, vertical and horizontal slices in Fig. 9(e) can contain all four colors, whereas in Fig. 8(d) they can only contain two colors. We believe that these more general double IETs generate *all* rectangle exchange transformations (RETs) [82], which cut the domain into a number of rectangles and recombine them after a set of translations.

In contrast to IETs, where it is easy to cut the line at arbitrary positions and rearrange the pieces according to an arbitrary permutation, it is significantly more difficult to cut the square into a given number of rectangles and rearrange them in a non-trivial way to recover the square. This problem is akin to the arbitrary cuts and shuffles that were discussed previously. For certain cases, "theorem-like" knowledge is available. For small numbers of rectangles (four or less), Haller has classified all possible RETs, and analyzed their mixing properties [82]. Other families of ergodic RETs can be constructed via "Pisot matrices" [83]. General double IETs provide a simple method to construct RETs with many pieces. However, it is not clear from the constituent IETs how many rectangular pieces will be created by a given general double IET. For example, it is difficult to construct an RET with exactly five rectangular pieces from a general double IET.

3.2.1. Extension to toroidal geometry — Non-PWI

Gluing the top and bottom edges of the square yields a cylinder, and then gluing the left and right edges produces a torus. The coordinate transformation from the square to the cylinder is an isometry, so PWIs on the square transform to PWIs on the cylinder. However, the coordinate transformation from the cylinder to the torus is *not* an isometry. To see that the coordinate transformation from the square to the torus is not an isometry, consider the map that moves tracers on the square vertically by half the square height. This is a simple translation (and, hence, isometry) on the square, but on the torus it amounts to rotation by 180° in the poloidal direction. The outer-most circle maps to the innermost circle, and so its length decreases, meaning the map is not an isometry. Hence, PWIs on the square are not PWIs on the torus, and vice versa

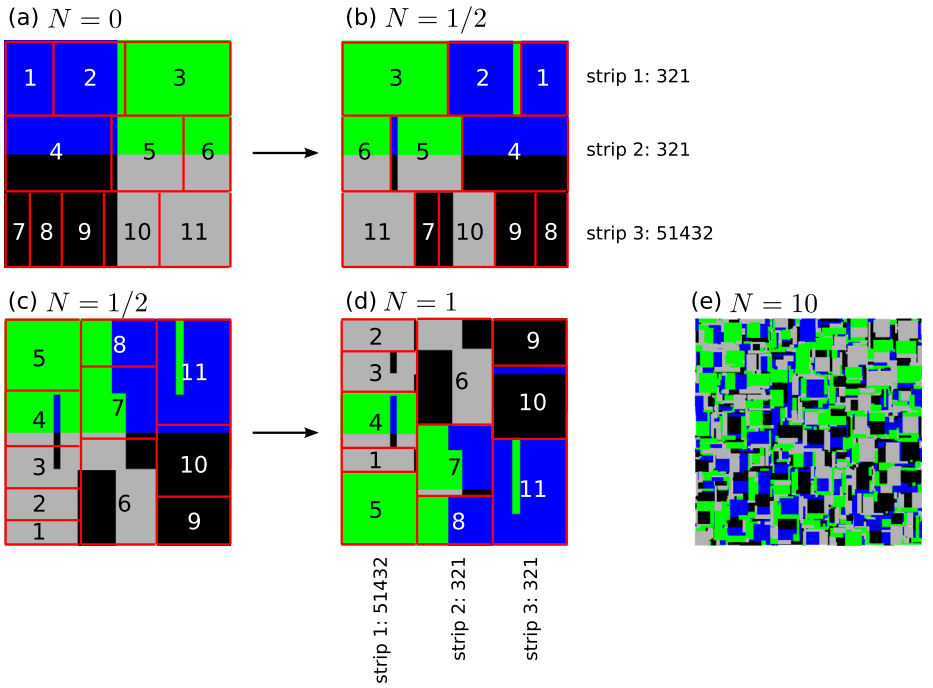

Fig. 9. More general double IET. First the square is divided into a number of horizontal strips (in this case three), and a different horizontal IET is performed on each horizontal strip [(a) → (b)]. In this case the first two strips use permutation 321, though with different cut locations, and the third strip uses permutation 51 432. Then the square is divided into a number of vertical strips (again three in this example), and different vertical IETs are performed on each vertical strip [(c) → (d)]. (d) After $N = 10$ iterations the colors become mixed, and mixing appears to be much better than the double IET shown in Fig. 8. In particular, vertical and horizontal slices can contain all four colors.

3.3. Overlapped planar wedge exchange transformations

The second embedding of IETs into 2D planar geometry shown in Fig. 4 is to view the 1D circle as having a non-zero radial width, i.e. as a 2D circular disk or annular version of the 1D circle. These are trivial "arc embeddings" of IETs into 2D planar geometry described by Ashwin et al. [81]. Cutting the circle amounts to cutting the annulus into wedges that are then rearranged. These planar wedge exchange transformations are similar to the cone exchange transformations studied by Ashwin and Goetz [36]. Planar wedge exchange transformations with a single annulus, as shown in Fig. 5(b), produce only 1D transport, because there is no transport in the radial direction. We can create 2D transport by considering an array of overlapped disks (or, equivalently, annuli), which breaks the rotational symmetry. Each disk successively undergoes a wedge exchange transformation, creating the potential for complex 2D transport and mixing. Fig. 10 shows a simple case where mixing is created by overlapping two disks with identical radii and alternately performing the wedge exchange transformation shown in Fig. 5(b) in each disk, which we call an "overlapped planar wedge exchange transformation". First the left disk is cut into three wedges, that are rearranged, as shown in Fig. 10(a). Then, the same transformation is applied to the right disk in Fig. 10(b). These two wedge exchanges form one iteration of the PWI. The second iteration is shown in Fig. 10(c, d). After 10 iterations, Fig. 10(e) shows that the red and white colors have become mixed. Of course, the disks can overlap to different degrees. In Fig. 10, the disks overlap by their radius r. Overlap of less than r results in mixing only at the periphery of each disk, with an unmixed region at the center of each disk. More general overlapped planar wedge exchange transformations can have more than two disks, e.g. an array of disks [Fig. 11(a, b)], and/or disks with different radii [Fig. 11(c, d)].

Also note that like IETs on a circle [Fig. 5(b)], planar wedge exchange transformations are generally not time-continuous PWIs. That is, the rearrangement cannot occur without extending the planar domain of the circles. There is one exception, which is the subject of the following section.

3.4. Overlapped disk rotations

The embedding of circle rotations into circle IETs, shown in Fig. 6, and discussed in Section 2.2, naturally extends (by thickening the width of the line in Fig. 5 circle) to an embedding of overlapped disk rotations into overlapped planar wedge exchange transformations. This is shown by the arrow from the 1D circle rotation class to the overlapped disk rotation class in Fig. 4.

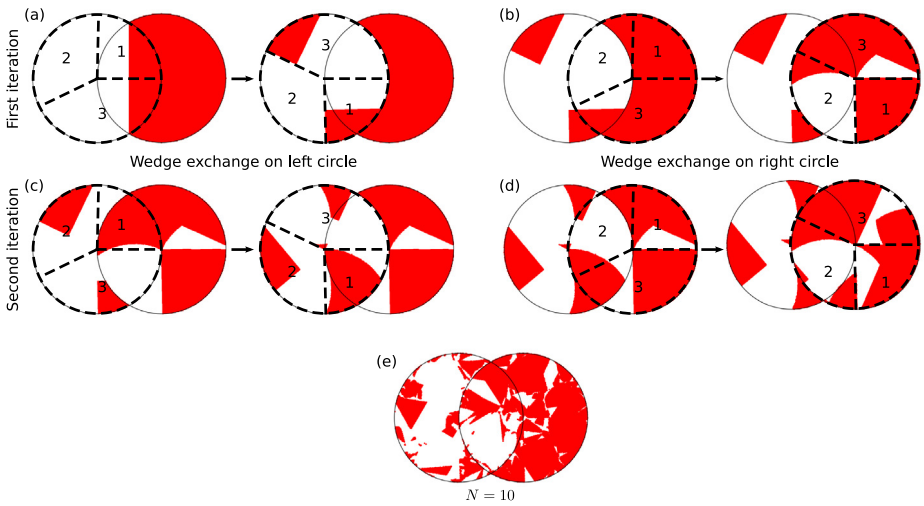

Fig. 10. Overlapped planar wedge exchange transformation for two overlapping disks. Each full iteration consists of a planar wedge exchange transformation of the left circle [shown in (a) and (c)], followed by a planar wedge exchange transformation of the right circle [shown in (b) and (d)]. The planar wedge exchange transformation is the same for both the left and right circles, which is the same as that used in Fig. 5(b). However, different transformations could be applied to each circle. (e) After 10 iterations the red and white colors become mixed.

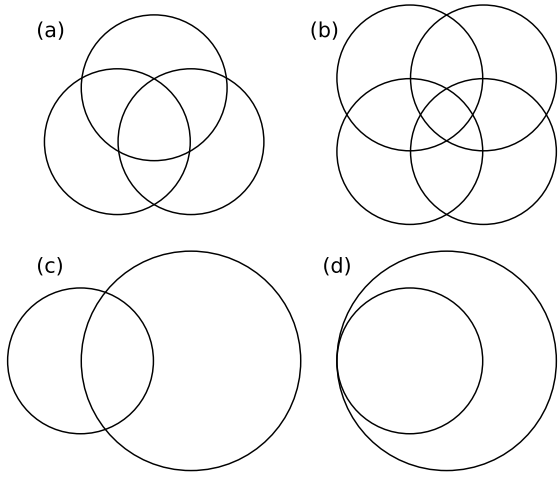

Fig. 11. Overlapped planar wedge exchange transformations can have more complex geometries than the two identical disk case shown in Fig. 10. For example, there can be more than two disks in an array, shown in (a) and (b), or disks with different radii and degrees of overlap, such as in (c) and (d).

One of the simplest cases for an overlapped disk rotation map consists of alternate rotation of two identical overlapped disks. This is demonstrated in Fig. 12. First, the left circle is rotated, as shown by the map from Fig. 12(a) to Fig. 12(b). In this example the left circle is rotated counter-clockwise by 125° with slip at its edge as indicated. To complete the PWI, the right circle is rotated clockwise by 125° again with slip at its edge, as shown by the map from Fig. 12(b) to Fig. 12(c). The second iteration of the PWI is shown in the steps from Fig. 12(c) to Fig. 12(d) to Fig. 12(e). After 10 iterations, Fig. 12(f) shows that even with this simple map, the red and white colors have become well mixed.

Practical implementations

Overlapped disk rotations do not cut and shuffle in the traditional sense, as occurs in IETs, RETs, and general planar wedge exchange transformations. Instead, discontinuous deformation is created by a "slip" deformation (known as a sliding singularity [66]) where the edge of the rotating disk meets the stationary disk. This means that the rotation of each disk in Fig. 12 can be represented as a time-continuous PWI. That is, pieces do not need to cross over other pieces to reach their new positions, as is needed for the actions in the general overlapped wedge exchange transformation, shown in Fig. 10. Instead, the action can be achieved by simple rotations while staying inside the domain. For this reason, many puzzles known as "twisty puzzles" have been designed based on this concept [84–89]. One of the first to be invented was the "Cohan Circle" puzzle [85], where two identical circles overlap by one radius. The circles are cut up into a number of

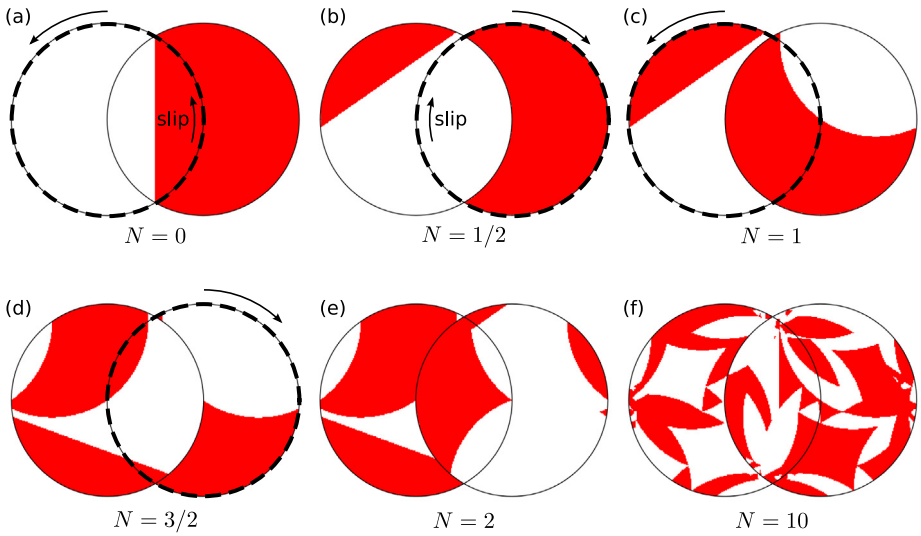

Fig. 12. Mixing produced by and overlapped disk rotation map. First, the left disk is rotated counter-clockwise by 125° [(a) maps to (b)], then the right disk is rotated clockwise by 125° [(b) maps to (c)]. This process is repeated from (c) to (e). (f) Mixing after 10 iterations.

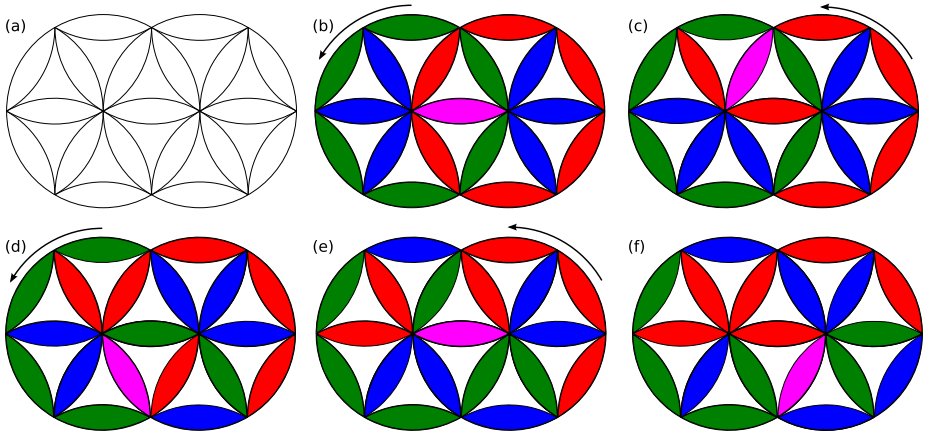

Fig. 13. Schematic of the Cohan circle puzzle (US patent 4580783, 1986) which was manufactured commercially and also marketed as the "Arusloky". (a) The configuration of pieces, with "petals" and "triangles". (b) The "solved" state. (c)–(f) Rotating counter-clockwise by 60° alternately about the centers of the left and right overlapped circles.

"petals" and triangles, as shown in Fig. 13(a), which are colored as shown in Fig. 13(b). The pieces are shaped such that the geometry shown in Fig. 13(a) is invariant under rotations of 60° about the center of each circle. This means the pieces can be scrambled by performing multiple 60° rotations, as demonstrated in Fig. 13(b–f), where we alternately rotate each circle counter-clockwise by 60°. Similar to the Rubik's cube, the aim is to return the puzzle to the solved state [Fig. 13(b)] after first scrambling the pieces.

Many generalizations of the Cohan Circle puzzle have since been created, including puzzles with more overlapping circles, circles with different sizes, and circles spaced more or less than one radius apart (see the "Museum" section of www.twistypuzzles.com for a comprehensive list). An important consideration is where the cuts in the disks need to be located for the puzzle to function (not jam). In the language of piecewise isometries, the cuts need to be located on the exceptional set [90], which is the set of all images and preimages of the discontinuities, i.e. points in the domain where cuts will eventually occur and points where cuts move to. For the exceptional sets shown in Fig. 14, gray regions will eventually be cut by the map, whereas white regions will never be cut. For identical circles whose centers are spaced one radius apart, alternately rotating by 60° (as in the Cohan Circle) yields the exceptional set shown in Fig. 14(a), which divides the domain into a finite number of pieces, which are the petals and triangles shown in Fig. 13(a). Note that three of the curves that define pieces of the Cohan circle [Fig. 13(a)] are missing from the exceptional set in Fig. 14(a). This

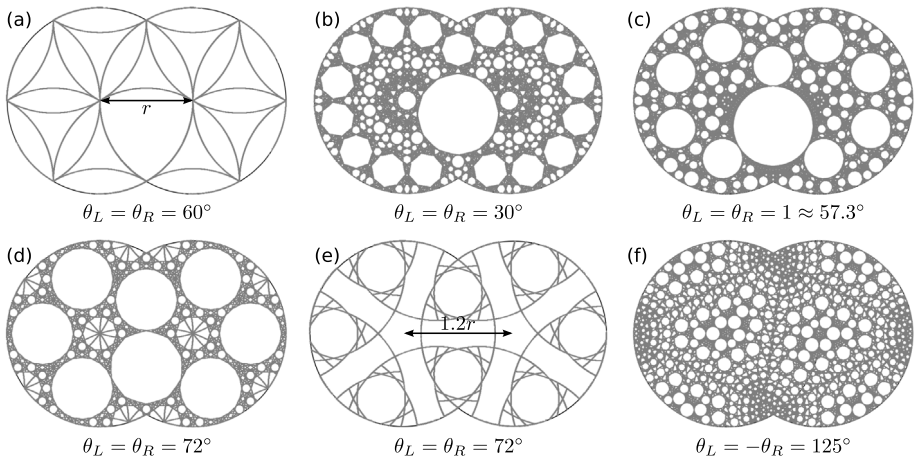

Fig. 14. Exceptional sets for the PWI generated by alternately rotating two overlapped disks. First, the left disk is rotated by θ_L, then the right disk is rotated by θ_R. In all cases the two disks are identical and spaced one radius, r, apart, except in (e) where they are spaced $1.2r$ apart. (a) For $\theta_L = \theta_R = 60°$, triangles and petals are formed, as in the Cohan circle puzzle. (b, c) For $\theta_L = \theta_R = 30°$, 57.3°, what appear to be complex fractal tilings are produced. (d) For $\theta = 72°$, when the disks are spaced r apart a fractal tiling is produced. (e) However, when the disks are sufficiently far apart, (e.g., $1.2r$) the exceptional set forms a finite polygonal tiling. (f) Rotations in opposite directions break the left–right symmetry of the exceptional set, as shown for $\theta_L = -\theta_R = 125°$, which is the same protocol as in Fig. 12.

is because the map does not consider every possible move of the puzzle, only alternate counter-clockwise rotations by 60°. In the puzzle, the disks can also be rotated clockwise, and through 120° and 180° as well, which accounts for these missing curves in the exceptional set.

The 60° case shown in Figs. 13 and 14(a) is special in that it only requires a finite number of pieces. In general, the disks would need to be cut into a fractal structure, i.e. infinitely many pieces, as demonstrated by the dense gray regions in Fig. 14(b–d,f). For puzzle-makers, a system with a fractal exceptional set, known as a "jumbling" puzzle, presents a challenge, because it is impossible to cut a solid disk into infinitely many pieces. This challenge can be overcome by "gluing" together infinitely many pieces, a practice known as "bandaging", so that only a finite number of pieces are required. Bandaging does however restrict the rotations that can be performed, since the puzzle will eventually jam. In contrast, for mixing applications with continuous, or fine-grained, media, a jumbling system is desirable, because the map will cut the media into smaller and smaller pieces that become mixed together. Note that whether a puzzle is jumbling or not, or equivalently whether the PWI is ergodic or periodic, is not determined solely by the two disk rotation angles, but also by the distance between the centers of the two overlapped disks. Consider $\theta_L = \theta_R = 72°$, when the distance between centers is one radius, r; the exceptional set is a fractal, as shown in Fig. 14(d). However, when the distance between centers is increased to $1.2r$, the exceptional set creates a finite polygonal tiling, as shown in Fig. 14(e). Clearly, there are a plethora of complex phenomena that occur in this simple system with two overlapped disks. For instance, when the rotations of the left and right disks are the same, the exceptional set has a left–right symmetry, observed in Fig. 14(a–e). However, that symmetry is broken when the rotation angles are different, as demonstrated by Fig. 14(f). Changing other geometric properties, such as the relative sizes of the circles or the number of circles (Fig. 11), would open up even more possibilities for transport and mixing within and between the circles.

Overlapped disk rotations have also been considered as a means to mix viscous fluids [47], where rotations are achieved by an array of helical flighted ducts in a larger flow channel. Each duct induces a rotation of the fluid within it, like the Kenics static mixer shown in Fig. 7. Abruptly changing the geometry of the array along the channel, from one configuration to another, allows the disk rotations to overlap, and mixing similar to Fig. 12 to take place. While this approach has been considered in the past – both conceptually and experimentally – this line of work seems to have stopped. The fact that overlapped disk rotation maps can be represented as time-continuous PWIs means that straight cylindrical ducts can be used. The ducts do not need to twist around each other to create mixing, unlike split-and-recombine mixers that emulate IETs and RETs, e.g., the design shown in Fig. 2. A similar principle has been implemented to mix granular materials [91].

3.5. Multi-axis lune exchange transformations

We have discussed two of the three embeddings of IETs into 2D geometries shown in Fig. 4. The third embedding is not into planar geometry, but into spherical geometry, as lune exchange transformations (when an orange is cut into wedges, the peel of a wedge is a lune). Instead of cutting the 2D disk into wedges, we cut the spherical shell into lunes, as shown in Fig. 15(a, b), and rearrange the lunes according to a permutation to reform the sphere, as shown in Fig. 15(c, d). Rearrangement of the lunes amounts to rotating each of them about a single axis, the line where all the cutting half-planes

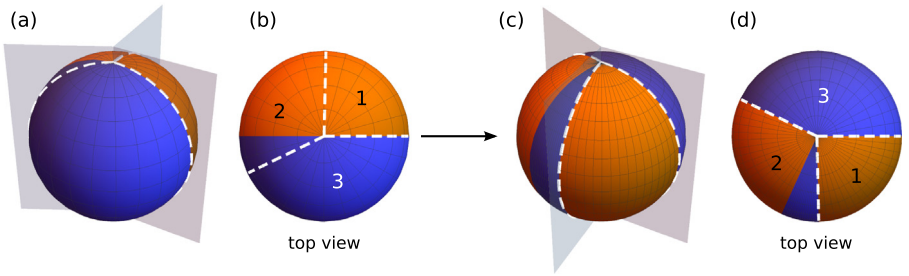

Fig. 15. Spherical lune exchange transformation. (a, b) The sphere, with one half colored orange and the other half colored blue is cut along the dashed white curves, where the sphere intersects three cutting half-planes, into three spherical lunes. (c, d) The lunes are rearranged by rotating them about the axis where the cutting half-planes intersect [the vertical axis in (a, c), the axis out of the page in (b,d)] to reassemble the sphere. The underlying IET defining the cuts and rearrangements is the same as in Fig. 5(b). To generate 2D transport, lune exchanges with different rotation axes must be used.

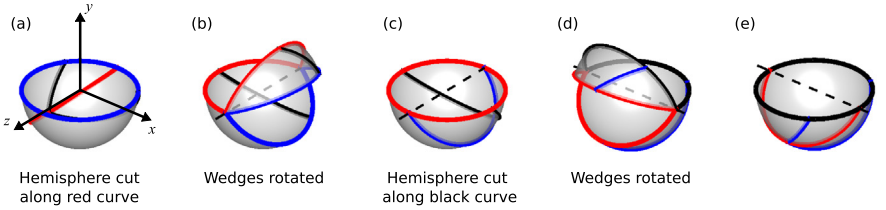

Fig. 16. The BST PWI as a (hemi)spherical lune exchange transformation. (a) The hemisphere is cut along the red curve, creating two lunes. (b) The lunes are rotated about the z-axis, by θ_z and $\theta_z + \pi$ respectively, to reform the hemisphere as shown in (c). (c) The hemisphere is cut along the black curve, creating two lunes. (d) The lunes are rotated about the x-axis, by θ_x and $\theta_x + \pi$ respectively, reforming the hemisphere as shown in (e). *Source:* Adapted with permission from Park et al. [41], Chaos **26**, 073115.

intersect [the vertical axis in Fig. 15(a, c), the axis out of the page in Fig. 15(b,d)]. Taking a cross-section of the sphere through any plane orthogonal to the rotation axis, the map is identical to a 1D IET of the circle, like that shown in Fig. 5(b). This clearly demonstrates the embedding of an IET. As a consequence, spherical lune exchange transformations with a single rotation axis only yield 1D transport. Tracers remain at the same latitude.

2D transport on the surface of the sphere can be generated by combining multiple lune exchange transformations, each having a different rotation axis. We call such a composition a "multi-axis lune exchange transformation". An example that has been studied extensively, both theoretically and experimentally, is the biaxial spherical tumbler (BST) PWI [13,37–43,45]. This is the system that motivated us to study mixing in PWIs. The map can be considered as the composition of two lune exchange transformations, using two perpendicular rotation axes. For the BST PWI, the upper hemisphere, $y > 0$ in Fig. 16[1], is invariant under both lune exchanges, so the domain of the BST PWI can be restricted to the lower hemisphere, where all the interesting dynamics take place. The physical reason for this restriction will be explained shortly. The action of the BST PWI on the lower hemisphere, $y \leq 0$, is shown in Fig. 16. First, a lune exchange transformation is performed using the z-axis as the rotation axis. The hemisphere is cut along the red curve to form two lunes, as shown in Fig. 16(a). The two lunes are rotated about the z-axis [Fig. 16(b)], by θ_z and $\theta_z + \pi$ respectively, to reform the hemisphere, as shown in Fig. 16(c). Then, a lune exchange transformation is performed using the x-axis as the rotation axis. The hemisphere is cut along the black curve to form two lunes, as shown in Fig. 16(c). The two lunes are rotated about the x-axis [Fig. 16(d)], by θ_x and $\theta_x + \pi$ respectively, to reform the hemisphere, as shown in Fig. 16(e). The composition of these two lune exchange transformations effectively cuts the hemisphere into the four partial lunes shown in Fig. 17(a), and rearranges them to reform the hemisphere as shown in Fig. 17(b). Varying the angles θ_x and θ_z changes the size of the lunes, which drastically changes the transport and mixing characteristics [41–43]. For example, some protocols have an exceptional set that is a fat fractal and covers almost the entire hemisphere, as shown in Fig. 17(c, d), indicating that most of the hemisphere will eventually be cut into arbitrarily small pieces which will be rearranged to yield good mixing. In contrast, there are special protocols, termed resonances [43], such that the exceptional set forms a finite polygonal tiling, as shown in Fig. 17(e). These resonances are similar to the exceptional sets for the overlapping circle PWIs shown in Fig. 14(a) and Fig. 14(e), where the map cuts the domain into a finite number of pieces. For these resonances, the entire domain is periodic, and mixing is generally poor.

[1] The vertical axis is y instead of z because the map is the 3D extension of a 2D map where y is vertical.

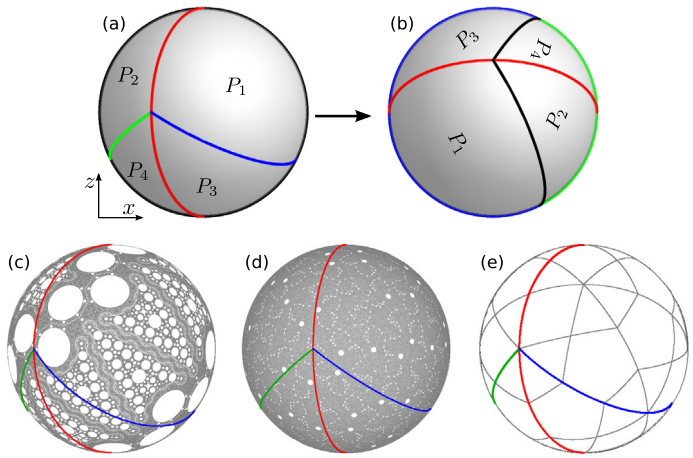

Fig. 17. The BST PWI cuts the hemisphere into the four partial lunes, P_{1-4}, shown in (a), and rearranges them as shown in (b). For most protocols the exceptional set has a fat fractal structure that covers a large portion of the hemisphere, such as in (c) where $\theta_z = \theta_x = 41.8°$, and (d) where $\theta_z = 45.8°$ and $\theta_x = 36.7°$. For a collection of special protocols, termed resonances, the exceptional set forms a finite polygonal tiling, such as in (d) where $\theta_z = \theta_x = 51.8°$.
Source: Adapted with permission from Smith et al., Phys. Rev. E, **95**, 062210 (2017).

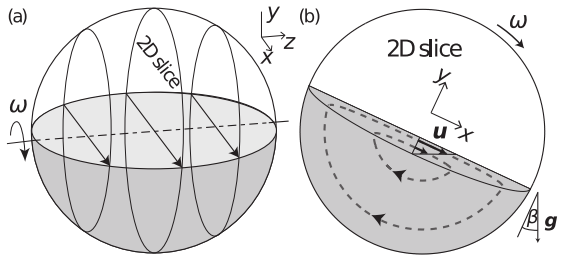

Fig. 18. Approximation of the flow of granular particles in a half-filled spherical tumbler. (a) For single axis rotation of granular material the flow can be approximated as a set of 2D circular slices, as the axial velocity component is quite small [93]. (b) The flow in one 2D slice. A particle in the bulk experience solid body rotation until it reaches the flowing layer at some position (x, y). Then the granular particle rapidly flows down the flowing layer, exiting at the reflected position $(-x, y)$.
Source: Used with permission from Zaman et al., Phys. Rev. E, **88**(1), 012208 (2013) [93].

Practical implementations

Another, more physical, interpretation of the BST PWI derives from the flow of granular media in a half-filled spherical tumbler that rotates alternately about two axes [38,39,45,92]. An approximation for the flow created by single axis rotation is shown in Fig. 18, with a "bulk" region that undergoes solid body rotation, and a thin flowing layer. In the limit of an infinitely thin flowing layer the flow is a time-continuous PWI. The infinitely thin flowing layer is equivalent to imposing a periodic boundary condition at the free surface — particles that reach the free surface are instantaneously reflected across it.

Switching the rotation axis, say to the x-axis as shown in Fig. 16(c–e), switches the periodic boundary condition (particles are reflected/rotated in a different direction). This switching results in discontinuous deformation that is neither a true cut-and-shuffle nor a slip deformation. Cutting occurs when a cluster of tracer particles partially crosses the periodic boundary when it switches. The periodic boundary splits the cluster into two clusters, which then move independently when the flow and periodic boundaries switch. In general, the two clusters remain separated, and will not reconnect. Essentially the same mechanism, switching periodic boundary conditions, is responsible for generating discontinuous deformations that occur in fluid flows driven by periodically reoriented extraction and reinjection wells [48–50,71–76]. Remarkably, it has been shown that features of the BST PWI, such as non-mixing regions, play a strong role in the transport, mixing, and pattern formation of granular particles in experiments [45,94].

For the BST PWI, the periodic boundary condition at the free surface means that the lune exchange transformation shown in Fig. 16 actually occurs as a time-continuous PWI of the hemisphere, which is why it can be implemented in experiments. However, more general lune exchange transformations are not time-continuous PWIs. The only exceptions

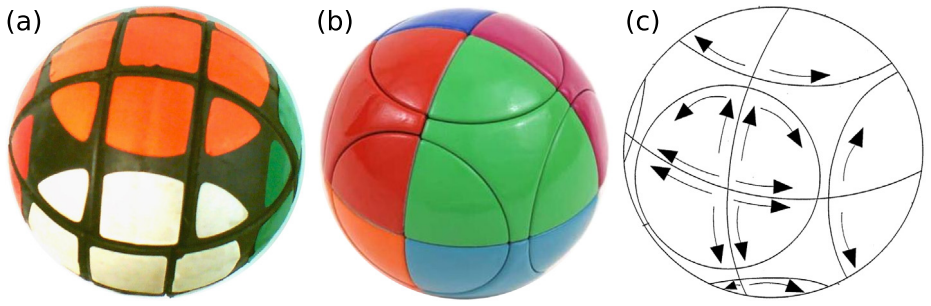

Fig. 19. (a) Rubik's sphere from Fig. 3, topologically equivalent to a $3 \times 3 \times 3$ Rubik's cube ©User:SpinningSpark / Wikimedia Commons/CC-BY-SA-3.0. (b, c) Marusenko sphere [97]. Hemispheres and smaller spherical caps can be rotated by 90°.

are uniform rotations of the sphere, which are uninteresting in isolation, but create complex 3D transport when coupled appropriately, as will be shown in Section 4.2.

3.6. Spherical cap rotations

Another fundamental piecewise-isometry on the sphere is rotation of a spherical cap. As with rotating overlapping disks in a plane (Fig. 12), spherical cap rotations are extensions of circle rotations (the top-most arrow in Fig. 4). Therefore, they produce discontinuous slip deformations, and they are time-continuous PWIs of the sphere. This means that the motion can be achieved without pieces crossing over one another, and, hence, the isometric motion can be theoretically applied to a solid sphere.

Practical implementations

There are several commercial twisty puzzles that utilize spherical cap rotations [95–97]. In fact, the most well known twisty puzzle, the Rubik's cube, utilizes spherical cap rotations, which becomes clear when the cube is transformed into the Rubik's sphere [shown in Fig. 19(a)]. Corner pieces on the Rubik's cube (with three colors) are triangles on the Rubik's sphere, edge pieces (with two colors) of the cube are rectangles on the sphere, and center pieces (with one color) of the cube are squares on the sphere. Twisting a face of the Rubik's cube is equivalent to rotating a spherical cap on the Rubik's sphere by 90°. A more recent puzzle based on spherical cap rotations is the Marusenko sphere [97], shown in Fig. 19(b, c). Two spherical cap rotations on a model of the Marusenko sphere are demonstrated in Fig. 20. First, the small cap at the top of the sphere is rotated by 90° [Fig. 20(b) mapping to Fig. 20(c)]; then the right hemisphere is rotated by 90° [Fig. 20(d) mapping to Fig. 20(e)].

For all twisty puzzles, the allowable spherical cap rotations are restricted by the existing "cuts" that separate pieces. Just like for a deck of cards, these physical restrictions mean there are only a finite number of states that can be reached. In contrast, general spherical cap rotations are not limited by these restrictions, such that any spherical cap can be rotated through any angle. Hence, general spherical cap rotations can theoretically cut the sphere into arbitrarily small pieces and yield good mixing. To demonstrate, consider the PWI introduced by Scott et al. [5,6], which is generated by spherical cap rotations and motivated by a "kicked" Hamiltonian. The action of the map is shown in Fig. 21. First the left and right hemispheres are counter-rotated [Fig. 21(a) mapping to Fig. 21(b)], then the entire hemisphere is rotated about the vertical axis [Fig. 21(c) mapping to Fig. 21(d)]. If the counter-rotation of the hemispheres and the rotation of the whole sphere are 90° or 180°, then the map cuts the domain into (at most) eight pieces (the eight colored octants shown in Fig. 21), and can be performed on the spherical analog of the $2 \times 2 \times 2$ Rubik's cube. However, Scott showed that for general rotation angles the exceptional set has a complex fractal structure, like that shown in Fig. 22 [5,6]. In these cases the sphere will be cut into infinitely many pieces.

Compositions of spherical lune exchange transformations and spherical cap rotations form a large class of easily parameterized spherical PWIs. In terms of practicality, all spherical cap transformations are time-continuous PWIs, which explains their prevalence in twisty puzzles such as the Rubik's sphere. In addition, using special periodic boundary conditions that approximate the motion of granular media in tumblers, the family of lune exchange transformations of the hemispherical shell that comprise the BST PWI are also time-continuous PWIs of the hemisphere. All other lune exchange transformations require pieces to overlap one another, and hence would be difficult to implement in any practical setting.

4. Three-dimensional cutting and shuffling

PWIs that generate 3D transport appear not to have been considered in the literature. As one would expect, the extension from 2D to 3D transport is far from straightforward. Here we briefly discuss two relatively simple systems with 3D cutting and shuffling to give a sense of the added complexity. However, more comprehensive studies are clearly required.

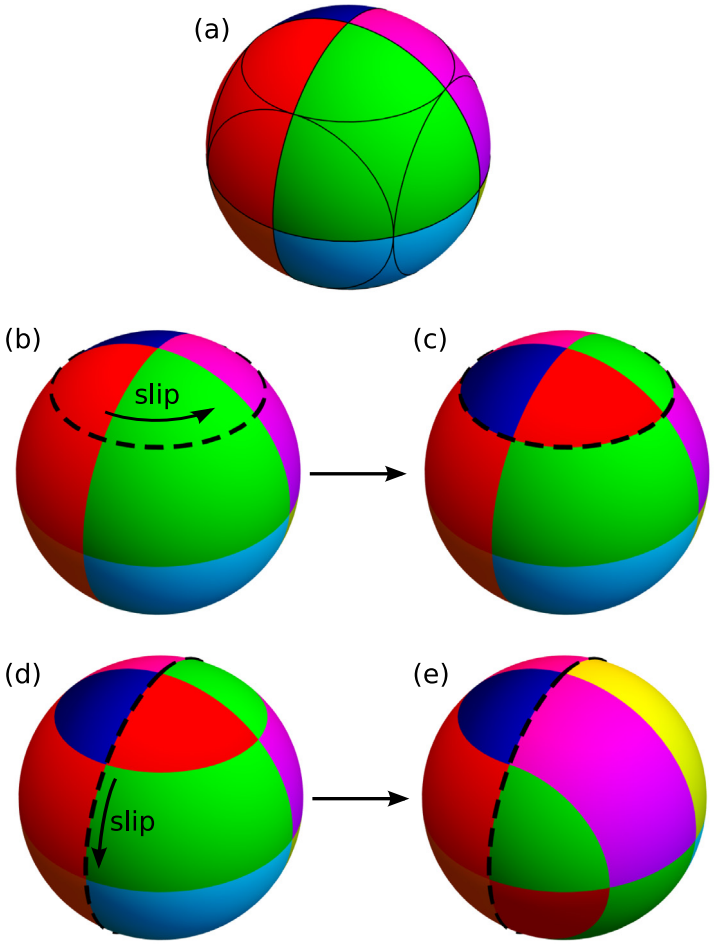

Fig. 20. Two spherical cap rotations on a model of the Marusenko sphere [Fig. 19(b, c)]. (a) The pieces of the Marusenko sphere. (b → c) The small cap at the top of the sphere is rotated by 90°. (d → e) The right hemisphere is rotated by 90°.

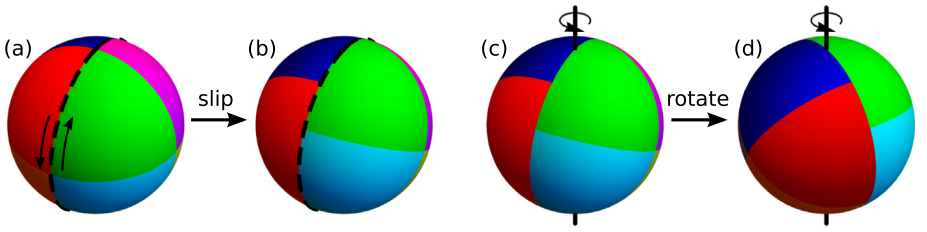

Fig. 21. Action of the PWI described by Scott et al. [5,6]. First, the left and right hemispheres are counter-rotated by angle μ (a → b), creating a discontinuous slip deformation. Then the entire sphere is rotated about the vertical axis by angle ω (c → d).

4.1. Cuboid exchange transformations

Similar to the extension of 1D interval exchange transformations to 2D rectangle exchange transformations, there is a natural extension to 3D cuboid exchange transformations of the cube. As is the situation for rectangle exchanges, it is generally difficult to cut a cube into arbitrary cuboids and non-trivially rearrange them to reform the cube. For example, there are 3D wooden cube puzzles where the aim is to reassemble a large cube from several smaller polycube pieces (each piece consists of multiple cubes glued together, like 3D Tetris pieces) [98]. It is challenging enough to try to reassemble the cube back to its starting configuration, let alone trying to find multiple solutions to the puzzle.

Like the double IETs in 2D, triple IETs that perform an IET in each of the three dimensions form a class of cuboid exchange transformations that are easy to construct and parameterize. An example is shown in Fig. 23, where the cube

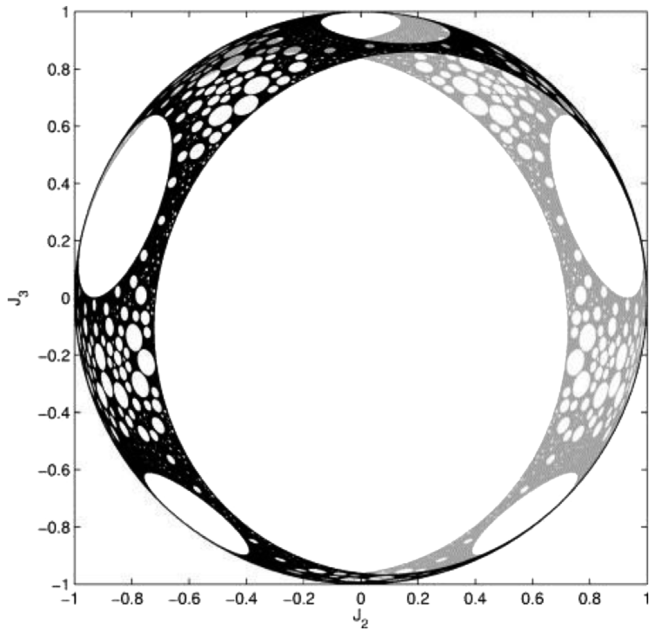

Fig. 22. Exceptional set for a spherical PWI composed of a spherical cap rotation and a rotation, as in Fig. 21 with $\mu = \omega = \pi(\sqrt{5} - 1)$ (see Scott et al. [5,6] for details).
Source: Used with permission from Scott, Physica D: Nonlinear Phenomena, **181**(1–2), pp. 45–52 (2003) [6].

is cut and shuffled in the x-direction [Fig. 23(a) → Fig. 23(b)], then in the y-direction [Fig. 23(c) → Fig. 23(d)], and then in the z-direction [Fig. 23(e) → Fig. 23(f)]. Triple IETs are extensions of IETs and double IETs, as shown by the connecting arrows in Fig. 4. Similar to double IETs, transport in triple IETs is limited. Material is not be able to mix between vertical or horizontal slices. In Fig. 23(g), each vertical or horizontal slice can only contain four colors. It is impossible for a slice to contain all eight colors. In addition, like double IETs and RETs, additional 3D space is needed to rearrange the pieces, so it is not a time-continuous piecewise-isometric motion.

Similar to the more general double IETs, demonstrated in Fig. 9, that we believe form the complete class of RETs, a more general class of triple IETs allow for different IETs to be performed on different sections of the cube. It is likely that this broader class of triple IETs encompasses all cuboid exchange transformations. This makes cuboid exchanges easier to define, and allows for a more systematic study of their properties.

4.2. Overlapped spherical PWIs

In the previous section we discussed spherical lune exchange transformations and spherical cap rotations, but for both types of PWI, particles are trapped on the surface of a 2D sphere. This is similar to planar wedge exchange transformations on a single disk, where tracers are trapped on a 1D circle. To generate 2D transport in the plane, we overlapped two disks and alternated between wedge exchange transformations in each disk, as shown in Figs. 10 and 12. The same strategy can be employed to generate 3D transport: overlapping spheres (now considered as 3D balls, i.e. the interior of the sphere is also included). The simplest case is two overlapped spheres, where the PWI is the composition of a rotation of each sphere, similar to the overlapped disk case with "slip" shown in Fig. 12. The resultant dynamics depends on several factors, including the geometries of the spheres (distance between centers and sphere radii), the rotation angles for the left (θ_L) and right (θ_R) spheres, and the rotation axes. The geometry of the rotation axes is critically important.

If the rotation axes are parallel, then there is no motion along the direction of the rotation axes. Therefore, tracers are trapped on planes orthogonal to the rotation axes, as demonstrated in Fig. 24(a, b) for spheres with identical radii having centers separated by one radius. In each plane orthogonal to the rotation axes, the map is identical to a 2D map with overlapped disks, like those shown in Figs. 12 and 14, with varying radii and degrees of overlap at each position along the axes. In particular, the map in the plane shown in Fig. 24(a) is the same as the map in Fig. 14(c). This clearly demonstrates the embedding of overlapped disk rotations into overlapped sphere rotations, shown by the connecting arrow in Fig. 4.

If the rotation axes are not parallel, but they intersect (when treated as lines that extend to infinity), then transport is still 2D. Tracers are trapped on spherical shells, where the center of all the shells is the point where the two rotation axes intersect. This is demonstrated by the examples in Fig. 24(c, d), where tracers are trapped on spherical shells concentric

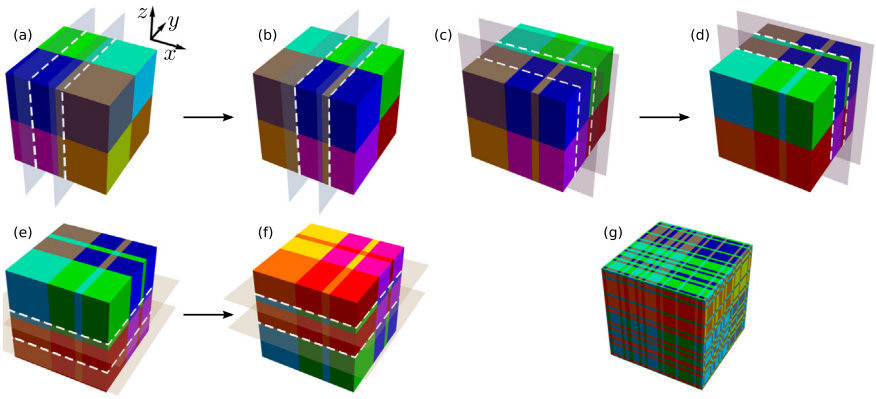

Fig. 23. Cuboid exchange transformation as a triple interval exchange transformation. An IET (the one shown in Fig. 5) with respect to each of the three axes. First, the cube is cut in the x-direction (cutting planes are orthogonal to the x-axis) into three cuboids, which are rearranged as shown in (a) → (b). The procedure is then repeated by cutting in the y-direction [(c) → (d)], and then in the z-direction [(e) → (f)]. (g) The cube after $N = 10$ iterations of the three-step procedure shown in (a)–(f).

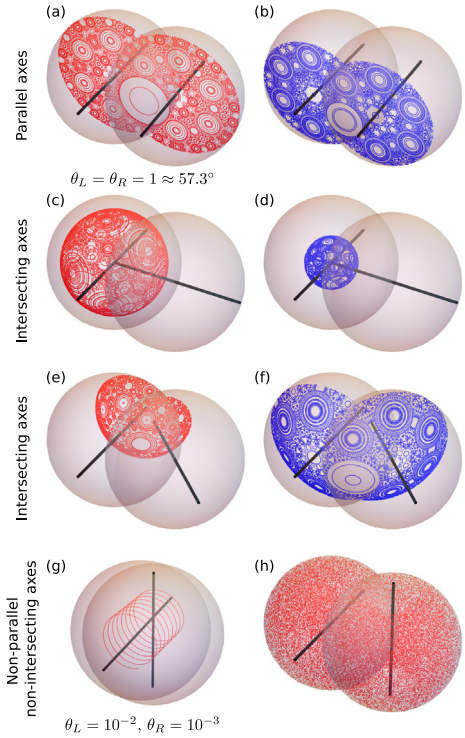

Fig. 24. Tracer trajectories for the PWI given by alternate rotations of two overlapped spheres. First tracers in the left sphere rotate by θ_L, then tracers in the right sphere rotate by θ_R, in both cases the rotation axes are shown as thick black lines. In every figure except (g), $\theta_L = \theta_R = 1 \approx 57.3°$, and the centers of the spheres are one radius apart. (a, b) For parallel rotation axes tracers are trapped on planes. Each figure shows the trajectories of 50 tracers (seeded randomly in a plane orthogonal to the rotation axes and within the two spheres) for 1000 iterations. (c–f) For intersecting rotation axes tracers are trapped on spherical shells. Each figure shows the trajectories of 50 tracers (seeded randomly on a single spherical shell centered at the point where the axes intersect and within the two spheres) for 1000 iterations. Note that in (e) and (f) the black lines indicating rotation axes do not intersect in the figure, but would intersect if they were extended to infinity. (g, h) For non-parallel, non-intersecting rotation axes, tracers in the region of intersection between the two spheres undergo screw motion, which leads to complex 3D transport. (g) The trajectory of one tracer for 5000 iterations with $\theta_L = 10^{-2}$, $\theta_R = 10^{-3}$, and the centers of the spheres spaced one fifth of a radius apart. Small angles are used to clearly illustrate the screw motion. (h) The trajectory of one tracer for 50,000 iterations explores a 3D volume.

with the left sphere, because the two rotation axes intersect at the center of the left sphere. For Fig. 24(e, f), the two rotation axes intersect at the point where the left axis meets the edge of the left sphere, which forms the center of the spherical shells. Of course, in this case the tracers cannot extend beyond the boundaries of the two spheres that make the domain, so the tracers do not cover the entire spherical shell as in Fig. 24(c, d). The reason tracers are trapped on spherical shells centered on the axes intersection point is that the distance from the intersection point does not change under either of the rotation maps, i.e. it is an invariant of the PWI.

The last case is non-parallel, non-intersecting rotation axes, which is arguably the most interesting for transport and mixing. The composition of rotations with non-parallel, non-intersecting axes does not generate another rotation, instead it generates a screw motion. That is, there is rotation about an axis, but also translation along that axis, termed pitch. Similar to translations in 1D, and rotations in 2D, screw motions are the most general rigid body transformation in 3D. For the overlapped sphere map, screw motion is most easily observed when the separation of the spheres is small and the rotation angles about each axis are also small, as shown in Fig. 24(g), where the centers of the spheres are spaced a fifth of a radius apart, $\theta_L = 10^{-2}$, and $\theta_R = 10^{-3}$. In this case, the screw axis is close to, but not the same as, the left rotation axis (horizontal). The screw motion persists as long as the tracer stays within the intersection of the two spheres. For example, the tracer particle undergoing a screw motion in Fig. 24(g) is trapped to a cylinder for the 5,000 iterations shown. However, it cannot screw along that cylinder indefinitely without exiting the domain. Instead, the tracer ceases its screw motion when it exits the region where the two spheres overlap. The tracer is then rotated about only one of the rotation axes, until it reenters the overlapped region and begins a similar screw motion, but possibly on a different cylinder. Therefore, particles may be trapped for long periods of time on screw cylinders but are able to jump between cylinders.

After a large number of iterations, the tracers visit the majority of the domain, although we have not explored this in detail. Three-dimensional transport clearly occurs for spheres whose centers are separated by one radius, with a rotation angle of 1 about each axis. Fig. 24(h) shows that one tracer explores almost the entire domain. This is in stark contrast to the cases shown in Fig. 24(a–f), where tracers are trapped on 2D surfaces.

The presence of screw motions opens up many new possibilities for transport and mixing in 3D PWIs. In 2D, tracers are generally either trapped to a 1D orbit in a cell, or are able to explore the ergodic region. In 3D, tracers may still be trapped on 1D curves, but they can also jump between screw cylinders. Preliminary evidence suggests that many other interesting phenomena are possible, including tracers transitioning between screw motions and ergodic motions on 2D surfaces.

A more general class of 3D PWIs consists of arrays of overlapping spheres, where the PWI is a composition of spherical lune/wedge exchange transformations and spherical cap rotations within each sphere. This broad class captures the dynamics of many different PWI classes, as shown by the multitude of connections leading to the general overlapped sphere PWI class in Fig. 4. The properties of general overlapped sphere PWIs will depend on the properties of the underlying lune exchanges and spherical cap rotations, as well as the orientations of the rotation axes, as for the two sphere case. In particular, rotation axes must be non-parallel and non-intersecting to yield screw motions.

5. Conclusions

We have presented a number of easily parameterizable cutting and shuffling motions for different geometries. In 1D, interval exchange transformations are the only form of cutting and shuffling, akin to shuffling a deck of cards. We have demonstrated natural extensions (embeddings) of IETs into 2D planar (as rectangle exchange transformations or wedge exchange transformations on overlapped disks), 2D spherical (as lune exchange transformations using multiple rotation axes), and 3D (as cuboid exchange transformations or wedge exchanges on overlapped spheres) geometries. We have also discussed spherical cap rotations, which are extensions of 1D circle rotations that can generate complex 2D transport when multiple rotation axes are used. Using compositions of these cutting and shuffling actions, large classes of PWIs can be constructed (Fig. 4) and their properties studied.

One property that we highlight is whether a cutting and shuffling motion can be represented as a time-continuous PWI. In other words, can the time-discrete map, which instantaneously transforms the domain, be expressed as a time-continuous motion that can be applied to a solid body without deforming or extending the domain? In 1D, the only PWIs with this property are rotations of the 1D circle, which naturally extend to rotations of disks in 2D planar geometry, and rotations of spherical caps in 2D spherical geometry. It is no coincidence that rotations of overlapped disks and spherical caps are the primary mechanisms that drive many twisty puzzles, such as the Cohan circle (Fig. 13, [85]), Rubik's sphere [Fig. 19(a)], and Marusenko sphere [Fig. 19(b, c), [97]]. A key limitation of twisty puzzles is that the domain must be pre-cut into a finite number of pieces, which restricts the allowable PWI parameters. In effect, the domain of a twisty puzzle is discrete. For continuous domains, parameter choices are essentially unlimited.

Another example of a time-continuous PWI is the biaxial spherical tumbler (BST) PWI [13,37–43,45]. In contrast to rotations of overlapped disks and spherical caps, where discontinuous deformations are created by slipping a moving piece over a stationary piece (known as sliding singularities [66]), the BST PWI generates discontinuous deformations by periodically changing a periodic boundary condition. The BST PWI has been studied extensively, since it approximates the flow of granular material in a half-filled spherical tumbler [38,39,45,92]. Unlike twisty puzzles, there are no restrictions on the parameter choices (the two rotation angles) of the BST PWI, because the domain is effectively continuous and can be cut into arbitrarily small pieces.

Note that our classification of cutting and shuffling maps shown in Fig. 4 is by no means complete. Our aim was to show the relationships between a number of easily parameterizable PWIs in different dimensions and geometries. More work is needed to form a complete classification, especially for 3D PWIs, which have not been studied previously. In this study we have only scratched the surface of cutting and shuffling in 3D.

Future work should also focus on understanding and classifying the transport and mixing characteristics of different classes of PWIs. Even the simplest form of cutting and shuffling, IETs, demonstrates rich transport and mixing phenomena. Similarly, complete classification of transport and mixing phenomena in other relatively simple geometries has been shown to be complex [32,82,99]. We expect that other, more complex, geometries will yield yet more interesting behavior.

Moreover, here we have considered systems with only cutting and shuffling. However, many interesting phenomena occur when cutting and shuffling is coupled with other transport mechanisms, such as stretching and folding [44,48,49,100] and/or diffusion [10,14,23,101,102]. These couplings should be studied in more detail and in more complex geometries.

Acknowledgment

P.B. Umbanhowar was partially supported by the National Science Foundation, USA, Contract No. CMMI-1435065.

References

[1] L.O. Chua, T. Lin, Chaos in digital filters, IEEE Circuits Syst. 35 (6) (1988) 648–658.
[2] P. Ashwin, Elliptic behaviour in the sawtooth standard map, Phys. Lett. A 232 (6) (1997) 409–416.
[3] P. Ashwin, W. Chambers, G. Petkov, Lossless digital filter overflow oscillations; approximation of invariant fractals, Int. J. Bifurcation Chaos 07 (11) (1997) 2603–2610, http://dx.doi.org/10.1142/S021812749700176X.
[4] J.H.B. Deane, Piecewise isometries: Applications in engineering, Meccanica 41 (3) (2006) 241–252, http://dx.doi.org/10.1007/s11012-005-5895-3.
[5] A. Scott, C. Holmes, G. Milburn, Hamiltonian mappings and circle packing phase spaces, Physica D 155 (1–2) (2001) 34–50, http://dx.doi.org/10.1016/S0167-2789(01)00263-9, URL http://www.sciencedirect.com/science/article/pii/S0167278901002639.
[6] A. Scott, Hamiltonian mappings and circle packing phase spaces: numerical investigations, Physica D 181 (1–2) (2003) 45–52, http://dx.doi.org/10.1016/S0167-2789(03)00095-2, URL http://www.sciencedirect.com/science/article/pii/S0167278903000952.
[7] J.M. Ottino, The Kinematics of Mixing: Stretching, Chaos, and Transport, Cambridge University Press, 1989.
[8] M. Keane, Interval exchange transformations, Math. Z. 141 (1) (1975) 25–31, http://dx.doi.org/10.1007/BF01236981.
[9] M. Keane, Non-ergodic interval exchange transformations, Israel J. Math. 26 (2) (1977) 188–196, http://dx.doi.org/10.1007/BF03007668.
[10] P. Ashwin, M. Nicol, N. Kirkby, Acceleration of one-dimensional mixing by discontinuous mappings, Physica A 310 (3–4) (2002) 347–363, http://dx.doi.org/10.1016/S0378-4371(02)00774-4, URL http://www.sciencedirect.com/science/article/pii/S0378437102007744.
[11] M.K. Krotter, I.C. Christov, J.M. Ottino, R.M. Lueptow, Cutting and shuffling a line segment: mixing by interval exchange transformations, Int. J. Bifurcation Chaos 22 (12) (2012) 1230041.
[12] M. Yu, P.B. Umbanhowar, J.M. Ottino, R.M. Lueptow, Cutting and shuffling of a line segment: Effect of variation in cut location, Int. J. Bifurcation Chaos 26 (14) (2016) 1630038, http://dx.doi.org/10.1142/S021812741630038X, URL http://www.worldscientific.com/doi/abs/10.1142/S021812741630038X.
[13] R. Sturman, The role of discontinuities in mixing, Adv. Appl. Mech. 45 (51) (2012) 51–90.
[14] G. Froyland, C. González-Tokman, T.M. Watson, Optimal mixing enhancement by local perturbation, SIAM Rev. 58 (3) (2016) 494–513, http://dx.doi.org/10.1137/15M1023221.
[15] M. Viana, Ergodic theory of interval exchange maps, Rev. Math. Comput. 19 (1) (2006) 7–100.
[16] W.A. Veech, Interval exchange transformations, J. Anal. Math. 33 (1) (1978) 222–272, http://dx.doi.org/10.1007/BF02790174.
[17] A. Katok, Interval exchange transformations and some special flows are not mixing, Israel J. Math. 35 (4) (1980) 301–310, http://dx.doi.org/10.1007/BF02760655.
[18] H. Masur, Interval exchange transformations and measured foliations, Ann. of Math. 115 (1) (1982) 169–200, URL http://www.jstor.org/stable/1971341.
[19] A. Avila, G. Forni, Weak mixing for interval exchange transformations and translation flows, Ann. of Math. (2007) 637–664.
[20] I.C. Christov, R.M. Lueptow, J.M. Ottino, Stretching and folding versus cutting and shuffling: An illustrated perspective on mixing and deformations of continua, Amer. J. Phys. 79 (4) (2011) 359–367.
[21] Y.G. Sinai, C. Ulcigrai, Weak mixing in interval exchange transformations of periodic type, Lett. Math. Phys. 74 (2) (2005) 111–133, http://dx.doi.org/10.1007/s11005-005-0011-0.
[22] L.D. Smith, P.B. Umbanhowar, J.M. Ottino, R.M. Lueptow, Optimized mixing by cutting-and-shuffling, SIAM J. Appl. Dyn. Syst. 17 (4) (2018) 2544–2573, http://dx.doi.org/10.1137/18M1176804.
[23] M. Wang, I.C. Christov, Cutting and shuffling with diffusion: Evidence for cut-offs in interval exchange maps, Phys. Rev. E 98 (2018) 022221, http://dx.doi.org/10.1103/PhysRevE.98.022221.
[24] C.F. Novak, Discontinuity-growth of interval-exchange maps, J. Mod. Dyn. 3 (3) (2009) 379–405, http://dx.doi.org/10.3934/jmd.2009.3.379, URL http://aimsciences.org/journals/displayArticlesnew.jsp?paperID=4474.
[25] A. Goetz, Dynamics of a piecewise rotation, Discrete Contin. Dyn. Syst. 4 (1998) 593–608.
[26] A. Goetz, et al., Dynamics of piecewise isometries, Illinois J. Math. 44 (3) (2000) 465–478.
[27] A. Goetz, Piecewise Isometries–An Emerging Area of Dynamical Systems, Birkhäuser, Basel, 2003.
[28] A. Goetz, M. Mendes, Piecewise rotations: bifurcations, attractors and symmetries, in: Bifurcation, Symmetry and Patterns, Springer, 2003, pp. 157–165.
[29] M. Boshernitzan, A. Goetz, A dichotomy for a two-parameter piecewise rotation, Ergodic Theory Dynam. Systems 23 (3) (2003) 759–770.
[30] A. Goetz, G. Poggiaspalla, Rotations by $\pi/7$, Nonlinearity 17 (5) (2004) 1787, URL http://stacks.iop.org/0951-7715/17/i=5/a=013.
[31] A. Goetz, A. Quas, Global properties of a family of piecewise isometries, Ergodic Theory Dynam. Systems 29 (2) (2009) 545–568.
[32] P. Ashwin, X.-C. Fu, On the geometry of orientation-preserving planar piecewise isometries, J. Nonlinear Sci. 12 (3) (2002) 207–240.
[33] P. Ashwin, X.-C. Fu, J.R. Terry, Riddling and invariance for discontinuous maps preserving lebesgue measure, Nonlinearity 15 (3) (2002) 633.
[34] P. Ashwin, A. Goetz, Invariant curves and explosion of periodic islands in systems of piecewise rotations, SIAM J. Appl. Dyn. Syst. 4 (2) (2005) 437–458, http://dx.doi.org/10.1137/040605394.

[35] P. Ashwin, A. Goetz, Polygonal invariant curves for a planar piecewise isometry, Trans. Amer. Math. Soc. 358 (1) (2006) 373–390.
[36] P. Ashwin, A. Goetz, Cone exchange transformations and boundedness of orbits, Ergodic Theory Dynam. Systems 30 (5) (2010) 1311–1330.
[37] R. Sturman, S.W. Meier, J.M. Ottino, S. Wiggins, Linked twist map formalism in two and three dimensions applied to mixing in tumbled granular flows, J. Fluid Mech. 602 (2008) 129–174, http://dx.doi.org/10.1017/S002211200800075X, URL https://www.cambridge.org/core/article/linked-twist-map-formalism-in-two-and-three-dimensions-applied-to-mixing-in-tumbled-granular-flows/45DCF7FCBD4E9312E3ECCE3AE5000F8E.
[38] G. Juarez, R.M. Lueptow, J.M. Ottino, R. Sturman, S. Wiggins, Mixing by cutting and shuffling, Europhys. Lett. 91 (2) (2010) 20003, URL http://stacks.iop.org/0295-5075/91/i=2/a=20003.
[39] G. Juarez, I.C. Christov, J.M. Ottino, R.M. Lueptow, Mixing by cutting and shuffling 3D granular flow in spherical tumblers, Chem. Eng. Sci. 73 (2012) 195–207, http://dx.doi.org/10.1016/j.ces.2012.01.044, URL http://www.sciencedirect.com/science/article/pii/S0009250912000632.
[40] I.C. Christov, R.M. Lueptow, J.M. Ottino, R. Sturman, A study in three-dimensional chaotic dynamics: Granular flow and transport in a bi-axial spherical tumbler, SIAM J. Appl. Dyn. Syst. 13 (2) (2014) 901–943, http://dx.doi.org/10.1137/130934076.
[41] P.P. Park, P.B. Umbanhowar, J.M. Ottino, R.M. Lueptow, Mixing with piecewise isometries on a hemispherical shell, Chaos 26 (7) (2016) 073115, http://dx.doi.org/10.1063/1.4955082.
[42] P.P. Park, T.F. Lynn, P.B. Umbanhowar, J.M. Ottino, R.M. Lueptow, Mixing and the fractal geometry of piecewise isometries, Phys. Rev. E 95 (2017) 042208, http://dx.doi.org/10.1103/PhysRevE.95.042208.
[43] L.D. Smith, P.P. Park, P.B. Umbanhowar, J.M. Ottino, R.M. Lueptow, Predicting mixing via resonances: Application to spherical piecewise isometries, Phys. Rev. E 95 (2017) 062210, http://dx.doi.org/10.1103/PhysRevE.95.062210.
[44] L.D. Smith, P.B. Umbanhowar, J.M. Ottino, R.M. Lueptow, Mixing and transport from combined stretching-and-folding and cutting-and-shuffling, Phys. Rev. E 96 (2017) 042213, http://dx.doi.org/10.1103/PhysRevE.96.042213.
[45] Z. Zaman, M. Yu, P.P. Park, J.M. Ottino, R.M. Lueptow, P.B. Umbanhowar, Persistent structures in a three-dimensional dynamical system with flowing and non-flowing regions, Nature Commun. 9 (3122) (2018) http://dx.doi.org/10.1038/s41467-018-05508-7.
[46] R. Spencer, R. Wiley, The mixing of very viscous liquids, J. Colloid Sci. 6 (2) (1951) 133–145, http://dx.doi.org/10.1016/0095-8522(51)90033-5, URL http://www.sciencedirect.com/science/article/pii/0095852251900335.
[47] C. Shearer, Mixing of highly viscous liquids: flow geometrics for streamline subdivision and redistribution, Chem. Eng. Sci. 28 (4) (1973) 1091–1098, http://dx.doi.org/10.1016/0009-2509(73)80012-0, URL http://www.sciencedirect.com/science/article/pii/0009250973800120.
[48] L.D. Smith, M. Rudman, D.R. Lester, G. Metcalfe, Mixing of discontinuously deforming media, Chaos 26 (2) (2016) 023113, http://dx.doi.org/10.1063/1.4941851, URL http://scitation.aip.org/content/aip/journal/chaos/26/2/10.1063/1.4941851.
[49] L.D. Smith, M. Rudman, D.R. Lester, G. Metcalfe, Localized shear generates three-dimensional transport, Chaos 27 (4) (2017) 043102, http://dx.doi.org/10.1063/1.4979666.
[50] S.W. Jones, H. Aref, Chaotic advection in pulsed source-sink systems, Phys. Fluids 31 (1988) 469–485.
[51] J. Branebjerg, P. Gravesen, J.P. Krog, C.R. Nielsen, Fast mixing by lamination, in: Proce. Ninth Int. Workshop Micro Electromech. Syst., 1996, pp. 441–446, http://dx.doi.org/10.1109/MEMSYS.1996.494022.
[52] B. Gray, D. Jaeggi, N. Mourlas, B. van Drieënhuizen, K. Williams, N. Maluf, G. Kovacs, Novel interconnection technologies for integrated microfluidic systems, Sensors Actuators A 77 (1) (1999) 57–65, http://dx.doi.org/10.1016/S0924-4247(99)00185-5, URL http://www.sciencedirect.com/science/article/pii/S0924424799001855.
[53] B. He, B.J. Burke, X. Zhang, R. Zhang, F.E. Regnier, A picoliter-volume mixer for microfluidic analytical systems, Anal. Chem. 73 (9) (2001) 1942–1947, PMID: 11354474, http://dx.doi.org/10.1021/ac000850x.
[54] M.S. Munson, P. Yager, Simple quantitative optical method for monitoring the extent of mixing applied to a novel microfluidic mixer, Anal. Chim. Acta 507 (1) (2004) 63–71, Microfluidics and Lab - On - a - Chip, http://dx.doi.org/10.1016/j.aca.2003.11.064. URL http://www.sciencedirect.com/science/article/pii/S0003267003015095.
[55] F. Schönfeld, V. Hessel, C. Hofmann, An optimised split-and-recombine micro-mixer with uniform 'chaotic' mixing, Lab. Chip 4 (1) (2004) 65–69.
[56] H. Chen, J.-C. Meiners, Topologic mixing on a microfluidic chip, Appl. Phys. Lett. 84 (12) (2004) 2193–2195, http://dx.doi.org/10.1063/1.1686895.
[57] D.S. Kim, S.H. Lee, T.H. Kwon, C.H. Ahn, A serpentine laminating micromixer combining splitting/recombination and advection, Lab. Chip 5 (2005) 739–747, http://dx.doi.org/10.1039/B418314B.
[58] H.M. Xia, S.Y.M. Wan, C. Shu, Y.T. Chew, Chaotic micromixers using two-layer crossing channels to exhibit fast mixing at low reynolds numbers, Lab. Chip 5 (2005) 748–755, http://dx.doi.org/10.1039/B502031J.
[59] A.P. Sudarsan, V.M. Ugaz, Multivortex micromixing, Proc. Natl. Acad. Sci. USA 103 (19) (2006) 7228–7233, http://dx.doi.org/10.1073/pnas.0507976103, URL http://www.pnas.org/content/103/19/7228.
[60] A. Schultz, I. Papautsky, J. Heikenfeld, Investigation of Laplace barriers for arrayed electrowetting lab-on-a-chip, Langmuir 30 (18) (2014) 5349–5356, http://dx.doi.org/10.1021/la500314v.
[61] T.P. Hunt, D. Issadore, R.M. Westervelt, Integrated circuit/microfluidic chip to programmably trap and move cells and droplets with dielectrophoresis, Lab. Chip 8 (2008) 81–87, http://dx.doi.org/10.1039/B710928H.
[62] J. Boujlel, F. Pigeonneau, E. Gouillart, P. Jop, Rate of chaotic mixing in localized flows, Phys. Rev. Fluids 1 (2016) 031301, http://dx.doi.org/10.1103/PhysRevFluids.1.031301.
[63] S.E. Boyer, D. Elliott, Thrust systems, AAPG Bull. 66 (9) (1982) 1196–1230.
[64] R. W.H.B.utler, The terminology of structures in thrust belts, J. Struct. Geol. 4 (3) (1982) 239–245, http://dx.doi.org/10.1016/0191-8141(82)90011-6, URL http://www.sciencedirect.com/science/article/pii/0191814182900116.
[65] T.H. Bell, Thrusting and duplex formation at mount isa, queensland, Australia, Nature 304 (5926) (1983) 493.
[66] B. Kahng, Singularities of two-dimensional invertible piecewise isometric dynamics, Chaos 19 (2) (2009) 023115, http://dx.doi.org/10.1063/1.3119464.
[67] G. Metcalfe, D.R. Lester, M.G. Trefry, A. Ord, Transport in a partially open porous media flow, in: Proc. SPIE 6802, Complex Systems II, vol. 6802, 2007, p. 68020I.
[68] D.R. Lester, G. Metcalfe, M.G. Trefry, A. Ord, B. Hobbs, M. Rudman, Lagrangian Topology of a periodically reoriented potential flow: Symmetry, optimization, and mixing, Phys. Rev. E 80 (2009) 036208.
[69] M.G. Trefry, D.R. Lester, G. Metcalfe, A. Ord, K. Regenauer-Lieb, Toward enhanced subsurface intervention methods using chaotic advection, J. Contam. Hydrol. 127 (2012) 15–29.
[70] H.A. Sheldon, P.M. Schaubs, P.K. Rachakonda, M.G. Trefry, L.B. Reid, D.R. Lester, G. Metcalfe, T. Poulet, K. Regenauer-Lieb, Groundwater cooling of a supercomputer in Perth, Western Australia: hydrogeological simulations and thermal sustainability, Hydrogeol. J. 23 (8) (2015) 1831–1849.
[71] B.A. Cola, Optimization of a Pulsed Source-sink Microscale Mixing Device (Ph.D. thesis), Vanderbilt University, 2004.
[72] B.A. Cola, D.K. Schaffer, T.S. Fisher, M. Stremler, et al., A pulsed source-sink fluid mixing device, J. Microelectromech. S. 15 (1) (2006) 259–266.
[73] A. Beuf, J.-N. Gence, P. Carrière, F. Raynal, Chaotic mixing efficiency in different geometries of hele-shaw cells, Int. J. Heat Mass Transfer 53 (4) (2010) 684–693.
[74] A.C. Bagtzoglou, P.M. Oates, Chaotic advection and enhanced groundwater remediation, J. Mater. Civ. Eng. 19 (1) (2007) 75–83.
[75] J.-M. Hertzsch, R. Sturman, S. Wiggins, DNA Microarrays: design principles for maximizing ergodic, chaotic mixing, Small 3 (2) (2007) 202–218.

[76] C.P. Schlick, A.B. Isner, P.B. Umbanhowar, R.M. Lueptow, J.M. Ottino, On mixing and segregation: From fluids and maps to granular solids and advection–diffusion systems, Ind. Eng. Chem. Res. 54 (42) (2015) 10465–10471, http://dx.doi.org/10.1021/acs.iecr.5b01268.
[77] C.Y. Wang, On the low-reynolds-number flow in a helical pipe, J. Fluid Mech. 108 (1981) 185–194, http://dx.doi.org/10.1017/S0022112081002073.
[78] F.H. Ling, X. Zhang, A numerical study on mixing in the kenics static mixer, Chem. Eng. Commun. 136 (1) (1995) 119–141, http://dx.doi.org/10.1080/00986449508936357.
[79] D. Hobbs, F. Muzzio, The kenics static mixer: a three-dimensional chaotic flow, Chem. Eng. J. 67 (3) (1997) 153–166, http://dx.doi.org/10.1016/S1385-8947(97)00013-2.
[80] E. Saatdjian, A. Rodrigo, J. Mota, On chaotic advection in a static mixer, Chem. Eng. J. 187 (2012) 289–298, http://dx.doi.org/10.1016/j.cej.2012.01.122.
[81] P. Ashwin, A. Goetz, P. Peres, A. Rodrigues, Embeddings of interval exchange transformations into planar piecewise isometries, 2018, arXiv preprint arXiv:1805.00245.
[82] H. Haller, Rectangle exchange transformations, Monatsh. Math. 91 (3) (1981) 215–232, http://dx.doi.org/10.1007/BF01301789.
[83] I. Alevy, R. Kenyon, R. Yi, A family of minimal and renormalizable rectangle exchange maps, 2018, arXiv preprint arXiv:1803.06369.
[84] D.A. Engel, Puzzle, US Patent 4,415,158, 1983.
[85] H. Cohan, Puzzle comprising overlapping circles with interchangeable components, US Patent 4,580,783, 1986.
[86] S. Bagdassarian, A. Bagdassarian, Method and device for generating a didisorder gegeometric figure to be rearranged into an ororder gegeometric figure, Patent WO 96/30097, 1996.
[87] O. Raschkov, Kreispuzzle, Patent DE29904348U1, 1999.
[88] H.-C. Ku, Entertainment device, US Patent 6,022,021, 2000.
[89] D.A. Engel, Puzzle with meshing gear sections, US Patent 7,309,064, 2007.
[90] X.-C. Fu, J. Duan, On global attractors for a class of nonhyperbolic piecewise affine maps, Physica D 237 (24) (2008) 3369–3376, http://dx.doi.org/10.1016/j.physd.2008.07.012, URL http://www.sciencedirect.com/science/article/pii/S0167278908002881.
[91] T. Simons, S. Bensmann, S. Zigan, H. Feise, H. Zetzener, A. Kwade, Characterization of granular mixing in a helical ribbon blade blender, Powder Technol. 293 (2016) 15–25, http://dx.doi.org/10.1016/j.powtec.2015.11.041, URL http://www.sciencedirect.com/science/article/pii/S0032591015301844.
[92] S.W. Meier, R.M. Lueptow, J.M. Ottino, A dynamical systems approach to mixing and segregation of granular materials in tumblers, Adv. Phys. 56 (5) (2007) 757–827, http://dx.doi.org/10.1080/00018730701611677.
[93] Z. Zaman, U. D'Ortona, P.B. Umbanhowar, J.M. Ottino, R.M. Lueptow, Slow axial drift in three-dimensional granular tumbler flow, Phys. Rev. E 88 (2013) 012208, http://dx.doi.org/10.1103/PhysRevE.88.012208.
[94] M. Yu, P.B. Umbanhowar, J.M. Ottino, R.M. Lueptow, Pattern formation in a fully-3d segregating granular flow, 2019, arXiv preprint arXiv:1901.02988.
[95] G. Obermair, Räumliches schiebespielzeug, Patent DE3204033A1, 1983.
[96] W.O. Gustafson, Manipulatable icosahedron toy, US Patent 4,474,376, 1984.
[97] F.-A.P. Cabeza, A.I. Marusenko, Toy comprising an improved three-dimensional puzzle, US Patent 7,784,791, 2010.
[98] D.G. Loveland, Puzzle with polycubes of distributed and low complexity for building cube and other shapes, US Patent 8,632,072 B2, 2014.
[99] X. Bressaud, G. Poggiaspalla, A tentative classification of bijective polygonal piecewise isometries, Exp. Math. 16 (1) (2007) 77–99, http://dx.doi.org/10.1080/10586458.2007.10128987.
[100] L.D. Smith, M. Rudman, D.R. Lester, G. Metcalfe, Impact of discontinuous deformation upon the rate of chaotic mixing, Phys. Rev. E 95 (2017) 022213, http://dx.doi.org/10.1103/PhysRevE.95.022213.
[101] H. Kreczak, R. Sturman, M.C.T. Wilson, Deceleration of one-dimensional mixing by discontinuous mappings, Phys. Rev. E 96 (2017) 053112, http://dx.doi.org/10.1103/PhysRevE.96.053112.
[102] C. Bordenave, Y. Qiu, Y. Zhang, Spectral gap of sparse bistochastic matrices with exchangeable rows with application to shuffle-and-fold maps, 2018, arXiv preprint arXiv:1805.06205.